Atmos. Chem. Phys. Discuss., 15, 21219–21269, 2015
www.atmos-chem-phys-discuss.net/15/21219/2015/
doi:10.5194/acpd-15-21219-2015

Atmospheric Chemistry and Physics Discussions
Open Access

Parameterization of oceanic whitecap fraction based on satellite observations

M. F. M. A. Albert[1], **M. D. Anguelova**[2], **A. M. M. Manders**[1], **M. Schaap**[1], and **G. de Leeuw**[1,3,4]

[1]TNO, P.O. Box 80015, 3508 TA Utrecht, the Netherlands
[2]Remote Sensing Division, Naval Research Laboratory, Washington, DC 20375, USA
[3]Climate Research Unit, Finnish Meteorological Institute, Helsinki, Finland
[4]Department of Physics, University of Helsinki, Helsinki, Finland

Received: 30 May 2015 – Accepted: 3 July 2015 – Published: 6 August 2015

Correspondence to: M. F. M. A. Albert (monique.albert@tno.nl)

Published by Copernicus Publications on behalf of the European Geosciences Union.

Abstract

In this study the utility of satellite-based whitecap fraction (W) values for the prediction of sea spray aerosol (SSA) emission rates is explored. More specifically, the study is aimed at improving the accuracy of the sea spray source function (SSSF) derived by using the whitecap method through the reduction of the uncertainties in the parameterization of W by better accounting for its natural variability. The starting point is a dataset containing W data, together with matching environmental and statistical data, for 2006. Whitecap fraction W was estimated from observations of the ocean surface brightness temperature T_B by satellite-borne radiometers at two frequencies (10 and 37 GHz). A global scale assessment of the data set to evaluate the wind speed dependence of W revealed a quadratic correlation between W and U_{10}, as well as a relatively larger spread in the 37 GHz data set. The latter could be attributed to secondary factors affecting W in addition to U_{10}. To better visualize these secondary factors, a regional scale assessment over different seasons was performed. This assessment indicates that the influence of secondary factors on W is for the largest part imbedded in the exponent of the wind speed dependence. Hence no further improvement can be expected by looking at effects of other factors on the variation in W explicitly. From the regional analysis, a new globally applicable quadratic $W(U_{10})$ parameterization was derived. An intrinsic correlation between W and U_{10} that could have been introduced while estimating W from T_B was determined, evaluated and presumed to lie within the error margins of the newly derived $W(U_{10})$ parameterization. The satellite-based parameterization was compared to parameterizations from other studies and was applied in a SSSF to estimate the global SSA emission rate. The thus obtained SSA production for 2006 of 4.1×10^{12} kg is within previously reported estimates. While recent studies that account for parameters other than U_{10} explicitly could be suitable to improve predictions of SSA emissions, we promote our new $W(U_{10})$ parameterization as an alternative approach that implicitly accounts for these different parameters and helps to improve SSA emission estimates equally well.

1 Introduction

There are many reasons why it is important to study whitecaps, not the least because they are still surrounded by significant uncertainties (de Leeuw et al., 2011). Whitecaps are the surface phenomenon of bubbles near the ocean surface. They form at wind speeds of around $3\,\mathrm{m\,s^{-1}}$ and higher, when waves break and entrain air in the water which subsequently breaks up into bubbles which rise to the surface (Monahan and Ó'Muircheartaigh, 1986; Thorpe, 1982). The estimated global average of whitecap cover, i.e. the fraction of the ocean surface covered with whitecaps, is 2 to 5 % (Blanchard, 1963). Being visibly distinguishable from the rough sea surface, whitecaps are the most direct way to parameterize the enhancement of many air–sea exchange processes including gas- and heat transfer (Andreas, 1992; Fairall et al., 1994; Woolf, 1997; Wanninkhof et al., 2009), wave energy dissipation (Melville, 1996; Hanson and Phillips, 1999), and the production of SSA particles (e.g., Blanchard, 1963, 1983; Monahan et al., 1983; O'Dowd and de Leeuw, 2007; de Leeuw et al., 2011), because all these processes involve wave breaking and bubbles.

Measurements of the whitecap fraction W are usually extracted from photographs and video images collected in situ from ships, towers, and air planes (Monahan, 1971; Asher and Wanninkhof, 1998; Callaghan and White, 2009; Kleiss and Melville, 2011). Whitecap fraction is commonly parameterized in terms of wind speed at a reference height of 10 m, U_{10}. Wind speed is the primary driving force for the formation and variability of W. Whitecap fraction predicted with conventional $W(U_{10})$ parameterizations show a large spread between reported W values (Lewis and Schwartz, 2004; Anguelova and Webster, 2006). Part of these variations is due to differences in methods of extracting W from still and video images. Indeed, the spread of W values has decreased in recently published in situ datasets as image processing improved and data volume increased (de Leeuw et al., 2011). However, an order-of-magnitude scatter of W values remains, suggesting that U_{10} alone cannot fully predict the W variability. Other factors such as atmospheric stability (often expressed in terms of air–sea temperature

ACPD
15, 21219–21269, 2015

Parameterization of oceanic whitecap fraction based on satellite observations

M. F. M. A. Albert et al.

difference), sea surface temperature (SST) or friction velocity (combining wind speed and thermal stability, e.g., Wu, 1988; Stramska and Petelski, 2003) have been indicated to affect whitecap fraction with implications for the SSA production. Thus, parameterizations of W that use different, or include additional (secondary), forcing parameters to better account for W variability have been sought (Monahan and Ó'Muircheartaigh, 1986; Zhao and Toba, 2001; Goddijn-Murphy et al., 2011).

An alternative approach to address the variability of W is to use whitecap fraction estimates from satellite-based observations of the sea state, because such observations provide long-term global data sets which encompass a wide range of meteorological and environmental conditions, as opposed to local measurement campaigns during which a limited variation of conditions is usually encountered. Brightness temperature T_B of the ocean surface measured from satellite-based radiometers at microwave frequencies has been successfully used to retrieve geophysical variables, including wind speed (Wentz, 1997; Bettenhausen et al., 2006; Meissner and Wentz, 2012). The feasibility of estimating whitecap fraction from T_B has also been demonstrated (Wentz, 1983; Pandey and Kakar, 1982; Anguelova and Webster, 2006). Anguelova et al. (2006, 2009) used WindSat data (Gaiser et al., 2004) to further develop the method of estimating W from T_B, and compiled a database of satellite-based W accompanied with additional variables.

Salisbury et al. (2013) showed that satellite-based W values carry a wealth of information on the variability of W. In particular, these authors showed that the global distribution of satellite-based W values differs from that obtained using a conventional $W(U_{10})$ parameterization with important implications for modeling SSA emissions in climate and chemical transport models (Salisbury et al., 2014). Salisbury et al. (2013) proposed a new $W(U_{10})$ parameterization in power law form using satellite-based W estimates over the entire globe for a full year. They derived wind speed exponents

ACPD
15, 21219–21269, 2015

which are approximately quadratic and linear for different data sets:

$$W_{10} = 4.6 \times 10^{-3} \times U_{10}^{2.26}; \quad 2 < U_{10} \leq 20\,\mathrm{m\,s^{-1}},$$
$$W_{37} = 3.97 \times 10^{-2} \times U_{10}^{1.59}; \quad 2 < U_{10} \leq 20\,\mathrm{m\,s^{-1}}, \tag{1}$$

where W is expressed in % and the subscripts denote the T_B frequencies used to obtain W. These exponents are significantly different from the cubic and higher wind speed dependences proposed by Monahan and O'Muircheartaigh (1980, hereafter MOM80):

$$W(U_{10}) = 3.84 \times 10^{-6} U_{10}^{3.41} \tag{2}$$

and Callaghan et al. (2008):

$$W = 3.18 \times 10^{-3} (U_{10} - 3.70)^3; \quad 3.70 < U_{10} \leq 11.25\,\mathrm{m\,s^{-1}}$$
$$W = 4.82 \times 10^{-4} (U_{10} + 1.98)^3; \quad 9.25 < U_{10} \leq 23.09\,\mathrm{m\,s^{-1}} \tag{3}$$

The reason for such differences is that Eqs. (2) and (3) were developed from data taken on a regional scale with U_{10} measured locally, while the data used by Salisbury et al. (2013) for Eq. (1) implicitly account for the influence of secondary factors on a global scale.

In this study we explore the utility of the satellite-based W values from a standpoint of predicting emission rates of SSA. Whitecaps are used as a proxy for the amount of bubbles at the ocean surface. When these bubbles burst, they generate sea spray aerosol droplets which in turn transform to SSA when they equilibrate with the surroundings (Blanchard, 1983). Bursting bubbles produce film and jet droplets, whereas at high wind speeds, exceeding about $9\,\mathrm{m\,s^{-1}}$, additional sea spray is directly produced as droplets which are blown off the wave crests. These spume droplets are larger than the bubble-mediated SSA droplets (Andreas, 1992). In this study we will focus on bubble-mediated production of sea spray.

Sea spray aerosols (SSA) are important for the climate system because, due to the vast extent of the ocean, SSA are amongst the largest aerosol sources globally and

ACPD
15, 21219–21269, 2015

provide a major contribution to the scattering of short-wave electromagnetic radiation (de Leeuw et al., 2011). Having high hygroscopicity, SSA particles are a source for the formation of cloud condensation nuclei (O'Dowd et al., 1999; Ghan et al., 1998) and as such influence cloud microphysical properties. Sea spray aerosol particles mainly consist of sea salt and, in biologically active regions, of organic matter in the submicron size range (O'Dowd et al., 2004; Facchini et al., 2008; Partanen et al., 2014). While residing in the atmosphere, SSA provide surface and volume for a range of multiphase and heterogeneous chemical processes (Andreae and Crutzen, 1997) thus contributing to the production of inorganic reactive halogens (Cicerone, 1981; Graedel and Keene, 1996; Keene et al., 1999; Saiz-Lopez and von Glasow, 2012); participating in the production or destruction of surface ozone (Keene et al., 1990; Barrie et al., 1988; Koop et al., 2000); and providing a sink in the sulfur atmospheric cycle (Chameides and Stelson, 1992; Luria and Sievering, 1991; Sievering et al., 1992, 1995).

The emission rate of SSA particles, i. e., the number of SSA particles produced per unit of sea surface area per unit time, needed in climate models and chemical transport models, is described by a sea spray source function (SSSF). The most commonly used SSSF (Monahan et al., 1986, referred hereafter as M86) – that estimates SSA generation by indirect, bubble-mediated mechanisms – is formulated in terms of the whitecap fraction, as defined in MOM80, and the production of SSA per unit whitecap:

$$\frac{\mathrm{d}F_0}{\mathrm{d}r} = 1.373 \cdot U_{10}^{3.41} \cdot r_{80}^{-3}(1 + 0.057 r_{80}^{1.05}) \times 10^{1.19\exp(-B^2)}, \quad (4)$$

where r_{80} is the droplet radius at a relative humidity of 80 % and the exponent B is defined as $B = (0.380 - \log r_{80})/0.650$.

Estimates of SSA production fluxes using the whitecap method still vary widely (Lewis and Schwartz, 2004). Possible ways to improve the performance of a whitecap-method based SSSF are: (i) to reduce the uncertainties in the size-resolved production flux $\mathrm{d}F/\mathrm{d}r_{80}$, for instance by including the organic matter contribution to SSA at submicron sizes (O'Dowd et al., 2004; Albert et al., 2012), and (ii) to reduce the uncertainties

ACPD
15, 21219–21269, 2015

in the parameterization of W to better account for its natural variability. Here we report on a study aiming at improving W.

Our approach involves three steps. We start with an assessment of the satellite-based W data on a global scale to evaluate the wind speed dependence of the whitecap fraction over as wide a range of U_{10} values as possible. In assessing the W database, we also evaluate the impact of an intrinsic correlation between W and U_{10}, which could have been introduced in the process of estimating W from T_B (Salisbury et al., 2013). Stepping on this assessment, we next consider variations of whitecap fraction on regional scales in order to gain insights into the influence of secondary factors in different locations during different seasons. In this second step, we use the results of our regional analyses to derive a new, globally applicable $W(U_{10})$ parameterization that incorporates a correction for the possible intrinsic correlation between W and U_{10}. Finally, the utility of the new $W(U_{10})$ parameterization is evaluated by using it to estimate SSA emission. The results of this study are compared to the $W(U_{10})$ parameterization of MOM80, Callaghan et al. (2008), Salisbury et al. (2013), and previous predictions of SSA emissions.

2 Methods

A new parameterization for the whitecap fraction is derived using satellite data which are described in Sect. 2.1. The data sets used, the approach to derive the new parameterization, and the method estimating SSA emission are described in Sects. 2.2–2.4.

2.1 Satellite-based estimates of whitecap fraction

Anguelova and Webster (2006) describe in detail the general concept of retrieving the whitecap fraction W from measurements of the brightness temperature T_B of the ocean surface by satellite-borne radiometers. The whitecap fraction estimates used in this study are obtained from the WindSat T_B data. Salisbury et al. (2013) describe the basic points of the retrieval algorithm (hereafter referred to as the $W(T_B)$ algorithm). Briefly, the algorithm obtains W by using measured T_B data for the composite emissivity of the ocean surface and modelled T_B data for the emissivity of the rough sea surface and areas that are covered with foam. Minimization of the differences between the measured and modelled T_B data in the $W(T_B)$ algorithm ensures minimal dependence of the W estimates on model assumptions and input parameters. The T_B algorithm has been updated with physics based models for the roughness and foam emissivities (Bettenhausen et al., 2006; Anguelova and Gaiser, 2013) replacing the simple, empirical models used in the initial implementation of Anguelova and Webster (2006). Additionally, an atmospheric model is used to provide the atmospheric correction for the retrieval of ocean surface T_B from the WindSat measurements at the top of the atmosphere.

Wind speed U_{10} is one of the required inputs to the atmospheric, roughness and foam models (Anguelova and Webster, 2006; Salisbury et al., 2013). Wind speed data come from the SeaWinds scatterometer on the QuikSCAT platform or from the Global Data Assimilation System (GDAS), whichever matches up better with the WindSat data in time and space within 25 km and 60 min; hereafter we refer to both QuikSCAT or GDAS wind speed values as U_{10} from QuikSCAT or $U_{10QSCAT}$. The use of $U_{10QSCAT}$ in the estimates of satellite-based W is anticipated to lead to some intrinsic correlation when/if a relationship between W and $U_{10QSCAT}$ is sought.

WindSat measures T_B at five microwave frequencies, ranging from 6 to 37 GHz. Because different microwave frequencies probe the ocean surface at different skin depths, they have different sensitivity to the thickness of the foam layer (Anguelova and Gaiser, 2011): with frequency increasing, the sensitivity to thinner foam layers increases. As a result, information on different stages of whitecap evolution can be obtained. In this study only two frequencies are used, 10 and 37 GHz. At 10 GHz, predominantly thick foam that is associated with initial, active wave breaking (stage A whitecaps, Monahan and Woolf, 1989) could be observed, while thinner foam layers associated with decaying (stage B) whitecaps, are detected only partially. Because 37 GHz frequency is more sensitive to thin foam patches, both active and decaying whitecaps can be observed,

ACPD
15, 21219–21269, 2015

Parameterization of oceanic whitecap fraction based on satellite observations

M. F. M. A. Albert et al.

resulting in a larger signal at 37 GHz because decaying foam covers a much larger area of the ocean surface than active whitecaps (Monahan and Woolf, 1989).

The $W(T_B)$ algorithm provides W values at satellite resolution of 50 km × 71 km. Both ascending and descending passes of the satellite platform are available, thus providing satellite data at a given spot on the Earth surface twice a day, in the morning and in the evening. The W values are gridded into a $0.5^\circ \times 0.5^\circ$ box together with the variables accompanying each W value, namely $U_{10QSCAT}$, SST from GDAS, time (average of the times of all samples falling in each grid cell), and statistical data generated during the gridding including the root-mean-square (rms) error, standard deviation, and count (the number of individual samples in a satellite footprint averaged to obtain the daily mean W for a grid cell).

2.2 Data sets

In this study, satellite-based estimates of whitecap fraction at 10 and 37 GHz are used in daily pairs of W and U_{10} values for each grid cell for the year 2006. Only W values for horizontal H polarization were considered because W is a surface feature and in radiometric experiments the sensitivity of H polarization to changes in wind, and thus to whitecap formation, was found to be larger than that of vertical V polarization (Anguelova and Webster, 2006; Anguelova et al., 2006). Figure 1 shows an example of the global W distribution from WindSat for a randomly chosen day. The figure shows that the daily data do not provide global coverage. Due to the high variability in both space and time, the daily W data cannot be interpolated to provide better coverage. Therefore, only the available data are used without filling the gaps for areas where data are lacking. This global data set was used to assess the wind speed dependence of W and devise a method to analyse regional variations (Sect. 3.1.1). The annual global W distributions show regions with either relatively low or relatively high numbers of valid data points, ranging from 100 to 300 data points per grid cell per year when both ascending and descending satellite passes are considered. Thus different regions were selected using two criteria, namely (i) consider regions with a high number of valid data points, and (ii) obtain a selection representative of both the Northern and Southern Hemispheres (NH and SH). In this way, 7 regions of interest were selected (Fig. 2). The coordinates of the selected regions are listed in Table 1, together with the corresponding number of samples, and range and mean values for wind speed and SST. Whereas regions 2–7 are all in the open ocean, region 1 was selected for its landlocked position to identify the effect of short fetches. Although region 7 has, regarding its size, a relatively low number of W samples compared to regions 1–6, it is included in the list to compensate for the otherwise limited representation of the Northern Atlantic Ocean. The results for this region could also show the degree to which the number of samples affects the information W can give.

Following the results of the global data set assessment (Sect. 3.1.1), for each selected region, scatterplots of the square root of W against U_{10} were generated, and the best linear fits were determined. For the seasonal dependences, scatterplots were generated using all available daily data per month, ranging from 22 to 31 days of data.

2.3 Approach to derive whitecap fraction parameterization

The assessment of the satellite-based estimates of whitecap fraction (Sect. 3.1) informs our decision how to most effectively use these data to improve a whitecap-method based SSSF. The questions we considered were, (1) why develop a $W(U_{10})$ parameterization instead of using satellite-based W data directly; and (2) how to account for the influence of secondary factors: explicitly, including them in the parameterization, e.g., $W(U_{10}$, SST, atmospheric stability, etc.) or implicitly. These questions are addressed below.

A major benefit of using satellite-based W data directly in an SSSF is that these data reflect the amount and persistence of whitecaps as they are formed by both primary and secondary forcing factors acting at a given location. This approach limits the uncertainty to that of estimating W from satellite measurements and does not add uncertainty from deriving an expression for $W(U_{10})$. However, such an approach would limit global predictions of SSA emissions to monthly values because a satellite-based W data set

ACPD
15, 21219–21269, 2015

does not provide daily global coverage; i.e., one would need data like that in Fig. 1 for at least two weeks (and more for good statistics) in order to have full coverage of the globe. Alternatively, a parameterization of whitecap fraction derived from satellite-based W data can provide daily estimates of SSA emissions using readily available wind speed daily data. Importantly, such a parameterization will be globally applicable because the whitecap fraction data cover the full range of meteorological conditions encountered over most of the world oceans. The availability of a large number of W data would ensure low error in the derivations of the $W(U_{10})$ expression.

Generally, to fully account for the variability of whitecap fraction, a parameterization of W would involve wind speed and the most important additional forcings explicitly (Anguelova and Webster, 2006; Salisbury et al., 2013), especially those readily available from either observations or meteorological forecasts, such as U_{10}, SST, etc. However, a parameterization requiring the use of many variables is not conducive for application in global modeling. Therefore, a derivation of a $W(U_{10})$ expression using data representative for a wide range of conditions, and thus implicitly accounting for secondary forcing, is justifiable. We therefore set out to develop a $W(U_{10})$ parameterization which accounts for the secondary factors by a suitable functional choice of the $W(U_{10})$ relationship. To obtain a globally applicable $W(U_{10})$ parameterization, we averaged the $W(U_{10})$ relationships derived for each of the considered regions and over all months (Sect. 2.2).

Ideally, when deriving a $W(U_{10})$ parameterization, the data for W and U_{10} should come from independent sources. The intrinsic correlation between W and U_{10} that might have arisen from the use of U_{10} from QuikSCAT in the estimates of W from T_B (Sect. 2.1), might affect the relationship between W and U_{10} developed here. To evaluate the effect of this intrinsic correlation, $U_{10QSCAT}$ is replaced with U_{10} from the European Centre for Medium range Weather Forecasting (ECMWF), which is considered to be a more independent source; note though that even the ECMWF data are generated by assimilating observational datasets (e.g., from buoys) in a coupled

ACPD
15, 21219–21269, 2015

atmosphere-wave model (Goddijn-Murphy et al., 2011). Besides ECMWF wind data, for consistency we also extracted ECMWF SST values to use later in our analysis.

An additional advantage of quantifying the correlation between U_{10} from QuikSCAT and U_{10} from ECMWF is the availability of the latter at 3 h intervals as compared to the availability of W–U_{10} pairs twice a day (Sect. 2.1). It is, therefore, preferred to derive a $W(U_{10})$ parameterization that is based on ECMWF wind speed data.

Quantifying the intrinsic correlation between W and U_{10} from QuikSCAT comes down to quantifying how closely U_{10} from QuikSCAT and U_{10} from ECMWF correlate, for which these two quantities needed to be matched in time and space. To speed up calculation processes, and because this already provides a statistically significant amount of data, only ascending satellite overpasses were used in the analysis. Wind speeds above $35\,\mathrm{m\,s^{-1}}$ were discarded.

2.4 Estimation of sea spray aerosol emissions

The newly formulated $W(U_{10})$ parameterization is applied to estimate the global annual coarse mode SSA emission with sizes r_{80} ranging from 1 to 10 µm. The particles in the coarse mode consist, to a good approximation, solely of sea salt, whereas, in biologically active regions, the sub-micron size range additionally includes organic material, with an increasing contribution as particle size decreases (Facchini et al., 2008). Since the organic mass fraction in sub-micron sea spray aerosol particles is still highly uncertain (Albert et al., 2012) only the coarse mode SSA emission is estimated. As suggested by Salisbury et al. (2014), the 37 GHz W data are more suitable to present the production of larger SSA particles than the 10 GHz data.

The emission of coarse mode SSA was calculated using a modeling tool (Albert et al., 2010), in which the $W(U_{10})$ parameterization of MOM80, as integrated in Eq. (4), was replaced with the newly derived globally applicable $W(U_{10})$ parameterization (Eq. 9). The resulting size-segregated droplet number emission rate was converted to mass emission rate using the approximation $r_{80} = 2r_d$, where r_d is the particle dry

Discussion Paper | Discussion Paper | Discussion Paper | Discussion Paper |

ACPD
15, 21219–21269, 2015

Parameterization of oceanic whitecap fraction based on satellite observations

M. F. M. A. Albert et al.

radius (e.g., Lewis and Schwartz, 2004; de Leeuw et al., 2011), and a density of dry sea salt of 2.165 $kg\,m^{-3}$.

3 Results

3.1 Assessment of satellite-based whitecap fraction data

3.1.1 Wind speed dependence from global data set

Figure 3 shows global W data estimated from WindSat measurements for March 2006 as function of $U_{10QSCAT}$, at 10 GHz (Fig. 3a) and 37 GHz (Fig. 3b). For comparison, the MOM80 relationship (Eq. 2) is also plotted in each figure. The 10 GHz data show far less variability than those at 37 GHz. At 37 GHz, the W values at a certain wind speed vary over a much wider range, with the strongest variability for wind speeds of 10–20 $m\,s^{-1}$. This supports the suggestion that other variables, in addition to U_{10}, influence the whitecap fraction, such as SST or sea state. Salisbury et al. (2013) quantify this variability.

The 10 GHz scatterplot does not show W values for wind speeds lower than about 2 $m\,s^{-1}$ because at these low wind speeds no active breaking occurs, as mentioned in the introduction. In contrast, at 37 GHz non-zero whitecap fraction values are retrieved at wind speeds $U_{10} < 2\,m\,s^{-1}$. Salisbury et al. (2013) suggested that the presence of foam on the ocean surface at these low wind speeds could be due to residual long-lived foam. This residual foam might be stabilized by surfactants, which increases its lifetime (Garrett, 1967; Callaghan et al., 2013). Another explanation could be biological activity (Medwin, 1977). However, there is not enough information currently to prove any of these conjectures.

In Fig. 4 the same data are plotted as in Fig. 3 but instead of the value of W we plot the square root of W vs. U_{10}, to weigh both axes evenly, and fit a linear relationship to

ACPD
15, 21219–21269, 2015

the resulting scatterplots:

$$\sqrt{W} = 0.01U_{10} - 0.011 \quad 10\,\mathrm{GHz} \tag{5}$$

$$\sqrt{W} = 0.01U_{10} + 0.019 \quad 37\,\mathrm{GHz} \tag{6}$$

with coefficients of correlation R^2 of 0.996 and 0.956, respectively. The $\sqrt{W(U_{10})}$ values at 10 GHz for wind speeds below $\sim 3\,\mathrm{m\,s^{-1}}$ were discarded in the analysis because, as shown in Fig. 4, the linear relationship breaks up at about this wind speed. However, either discarding or taking into account these data points, does not significantly influence the position of the linear fit.

The quadratic trends of W with U_{10} in Fig. 4 are in contrast to the known cubic and higher wind speed dependences such as in the MOM80 relationship. Using satellite W data therefore results in a higher estimate of W at wind speeds lower than about $10\,\mathrm{m\,s^{-1}}$ (based on Fig. 3a, obtained with 10 GHz data) and about $15\,\mathrm{m\,s^{-1}}$ (based on Fig. 3b, with 37 GHz data), and a lower estimate for higher wind speeds. Wind speeds are generally lower than 10 or $15\,\mathrm{m\,s^{-1}}$ (cf. Fig. 3) and thus a $W(U_{10})$ parameterization based on these data will most of the time lead to higher W estimates than those obtained from using the MOM80 relationship.

3.1.2 Regional and seasonal variations

Figure 5 shows examples of the square root of W against $U_{10\mathrm{QSCAT}}$ for different regions and seasons. Figure 5a–b shows scatter plots retrieved over the Gulf of Mexico (region 1) at both frequencies for January 2006. Statistics are presented at the top of the figures and the fit lines are shown in red. Figure 5c–d shows the fit lines $\sqrt{W(U_{10})}$ for 10 and 37 GHz in region 5 for all months, while Fig. 5e–f demonstrates variations of the fit lines $\sqrt{W(U_{10})}$ for both frequencies over all regions for March 2006.

Figure 5 shows that the variations of the $\sqrt{W(U_{10})}$ relationships at 10 GHz are smaller than those for 37 GHz, confirming the same observation reported by Salisbury et al. (2013) but obtained with a different analytical approach. Focusing on the results for 37 GHz, Fig. 5d and f shows that geographic differences from region to region for a fixed time period yield more variability in the $\sqrt{W(U_{10})}$ relationship than seasonal variations at a fixed location, even for a location like region 5 where extreme seasonal changes could be observed. The standard deviation of the slopes in Fig. 5d is 3×10^{-4}, while that in Fig. 5f is 4×10^{-4}. We surmise that obtaining whitecap fraction data at different locations can ensure a wider range of meteorological and oceanographic conditions that influence W than data at a fixed location for different seasons. This suggests that extreme yet sporadic seasonal values of the major forcing factor such as U_{10} at a given location contribute less to the W variations than varying environmental conditions from different locations. Such observation has implications for collecting W data with the purpose of capturing and parameterizing the natural variability of whitecap formation and extent. For example, even if twice a day, satellite-based observations of W on a global scale are still an effective way to record influences of secondary factors. For in situ data collection, as could be expected, long-leg cruises would provide more information on the effect of secondary factors, while long-term monitoring at a specific location will be more suitable to capture the wind speed effect alone.

Though noticeable, overall Fig. 5 shows small variations: the slopes of the resulting $\sqrt{W(U_{10})}$ parameterizations for 12 months for all regions are found to be similar for all determined fits, about 0.01 with a standard deviation of 3×10^{-4}. Sampling differences between the regions (e.g., fewer samples in region 7 than in any other region) do not seem to cause significant differences between the resulting $\sqrt{W(U_{10})}$ fits. Also, the results from region 1 do not noticeably differ from the results from the other regions, or at least are within the spread of the different results. These outcomes do not provide sufficient information to draw conclusions on effects of short fetches. These small variations in the derived wind speed dependences across retrieval frequency, season, or location is in contrast to our expectation to reveal influences of environmental factors other than wind speed on W, in particular SST which influences viscosity. However, the high correlation coefficients suggest that U_{10} explains the variation in W to a very large extent. One possible explanation is that the additional influences have already been accounted for, at least partially, by using a quadratic power law. That is, the change from cubic to quadratic law is the change that the additional parameters impart on the $W(U_{10})$ relationship. Another suggestion might be that space and time variations of the secondary factors exist, but because they affect W in opposite ways (e.g., Monahan and O'Muircheartaigh, 1986), these influences cancel each other. Hence no further improvement can be expected by looking at effects of other factors on the variation in W explicitly, especially when the $W(U_{10})$ dependence is derived from a database covering a wide range of conditions.

In contrast to the slope result, the intercept (i.e., the value for W at zero wind speed, hereafter referred to as residual W) obtained with the 37 GHz W data shows strong variability (Fig. 6), with a mean value of 0.019, and a standard deviation of 0.004. These intercept variations at 37 GHz quantify the variations in absolute values of W by region and season seen in Fig. 5d and f. The intercepts that were obtained with the 10 GHz data show much less variability with a mean value of −0.011 and a standard deviation of 9×10^{-4}. Therefore, whereas 10 GHz data mainly provide the wind speed dependence of W, the 37 GHz data set provides information useful to quantify the influence of secondary factors on W, such as SST, the presence and amount of surfactants, or the local relaxation time of foam, depending on conditions like viscosity (Salisbury et al., 2013).

These conditions are not only determined by the actual circumstances but also by the processes through which they developed, i.e. the history of environmental and meteorological quantities at a certain location, such as rising or waning winds, or the amount of foam that was already present as discussed in Sect. 3.1.1.

Although the intercept at 10 GHz has no physical meaning on its own, one can learn from its behaviour: because the intercept, as well as the slope, hardly changes in time or space, the scatterplot as a whole is almost static. From this we can conclude that knowing the wind speed variation is enough to predict the new foam formation no matter whether these variations are caused by seasonal or geographical variations. Con-

ACPD
15, 21219–21269, 2015

sidering that W values at 10 GHz are representative of predominantly active whitecaps, it is plausible to assume that new foam formation is less, if at all, affected by varying secondary environmental factors.

Because only the 37 GHz data provide information that represents different conditions on the globe, the remainder of the data analysis in this study will be based on only these data.

The results in Fig. 6 show a higher seasonal variability as the latitudinal distance from the Equator increases. This might point at some correlation with water temperature. Therefore, using the SST data for all months of 2006 at three regions extracted from the ECMWF database, the regionally averaged SST profiles are shown in Fig. 7 together with the matching residual W. Figure 7 indicates that residual W and temperature are anti-correlated: with temperature increasing, the residual W roughly decreases. We discuss these results further in Sect. 4.

3.2 Parameterization of whitecap fraction

A parameterization of W in terms of U_{10} was obtained by averaging the $\sqrt{W(U_{10})}$ relationships for each region and for all months of 2006. The thus obtained relationship is similar to that derived from the global data set for only one month (Eq. 6):

$$\sqrt{W} = 0.01U_{10} + 0.020. \tag{7}$$

The method used to quantify the intrinsic correlation between W and U_{10} from QuikSCAT is described in Sect. 2.3. Figure 8 shows all ECMWF wind speed data that have been matched in time and space with the available $U_{10\mathrm{QSCAT}}$ data for March 2006. The majority of the data is clustered in the range of 5–10 m s^{-1}. The correlation between U_{10} from ECMWF ($U_{10\mathrm{ECMWF}}$) and U_{10} from QuikSCAT was determined as the best linear fit, forced through zero:

$$0.952 \cdot U_{10\mathrm{QSCAT}} = U_{10\mathrm{ECMWF}} \rightarrow U_{10\mathrm{QSCAT}} = 1.050 \cdot U_{10\mathrm{ECMWF}}, \tag{8}$$

ACPD
15, 21219–21269, 2015

Parameterization of oceanic whitecap fraction based on satellite observations

M. F. M. A. Albert et al.

with $R^2 = 0.844$. On average, U_{10} from ECMWF is about 5 % lower than U_{10} from QuikSCAT.

We cast Eq. (7) in terms of $U_{10\mathrm{ECMWF}}$ by combining it with Eq. (8). This allows for correction of the possible intrinsic correlation between W and U_{10}, which is applied in the resulting $W(U_{10})$ parameterization:

$$W = \left(U_{10\mathrm{ECMWF}}^2 + 4U_{10\mathrm{ECMWF}} + 4\right) \times 10^{-4}. \tag{9}$$

This newly derived W parameterization is compared to the MOM80 parameterization (Eq. 2) in Fig. 9, which shows the global annual average W distributions for 2006 obtained with Eqs. (2) and (9) and wind speeds from ECMWF. The MOM80 relationship yields a wider W range with higher values in regions with the highest wind speeds, as expected (see Sect. 3.1.1). In particular, this occurs over the southern oceans between about 40 and 70° S and in the North Atlantic between about 40 and 70° N. The latitudinal variations from the Equator to the poles are more pronounced when using the MOM80 relationship as compared to Eq. (9). The new $W(U_{10})$ parameterization provides a global spatial distribution with similar patterns, but the absolute values are lower at high latitudes and higher at low latitudes.

3.3 Sea spray aerosol production

The newly derived parameterization was used to estimate how it affects the global annual average emission of coarse mode sea spray aerosol (Fig. 10). The spatial distributions of the mass emission rates obtained with the new and the MOM80 $W(U_{10})$ parameterizations mimic the patterns of the W distributions shown in Fig. 9. This is expected because the M86 SSSF does not introduce variables that have a global pattern: the new $W(U_{10})$ parameterization determines the spatial distribution whereas the M86 SSSF provides the factor to multiply with (3.575×10^5).

Figure 11 shows the difference between the distributions of SSA mass emission rate. The annual emission rate calculated with the new $W(U_{10})$ parameterization (Eq. 9) is

ACPD
15, 21219–21269, 2015

about 40 % larger than that calculated with MOM80 (Eq. 2), giving higher emission rates over a large part of the globe. Specifically, the total supermicron SSA mass emission for 2006 is 2915 Tg (2.9×10^{12} kg) when using the MOM80 W parameterization, and 4082 Tg (4.1×10^{12} kg) when using Eq. (9).

4 Discussion

4.1 Assessment of satellite-based whitecap fraction data

The choice to use W data that were obtained at two different frequencies has led to more insight about the different stages of W. Based on the findings obtained with 10 GHz data, it can be concluded that for stage A whitecaps, for open ocean, the only real forcing factor is U_{10}, which mostly drives the absolute value of W with little variations caused by other factors. Following from the analysis of the 37 GHz data, more information was obtained on stage B whitecaps, namely that the amount of stage B whitecaps also clearly depends on the wind speed, but effects of other factors contribute to larger variations of the absolute values.

When taking a closer look at the data cloud distributions of the scatterplots in Figs. 3 and 4, one can notice that the 10 GHz data show a relatively sharp cut-off on the bottom side of the data cloud whereas for the 37 GHz data one can see a sharp cut-off on the upper side. This might imply that at a certain wind speed there is a clear minimum of W produced by active wave breaking, and a well set maximum of the total sum of W. Apparently at a certain wind speed only up to a certain amount of foam can exist. One could speculate on foam stability maxima constrained by wind speed but it should be considered that this might as well be an artifact of the $W(T_B)$ algorithm.

Considering our analyses of the W data sets, a lot seems to be explained by U_{10}. Although not very significant compared to those that are U_{10}-related, we do find some additional features as described below.

ACPD
15, 21219–21269, 2015

First, Fig. 3 (the same applies for Fig. 5, showing data on regional scale) shows that at both 10 and 37 GHz a larger spread in W data is observed at higher wind speeds. Based on their different penetration depths, 10 GHz feels active (stage A) and only partially residual (stage B) whitecaps, while 37 GHz reacts on all, stage A and B whitecaps. However, we can expect that the situation would change for 10 GHz as wind increases and with that the intensity and scale of the breaking waves. Because larger breakers form larger and deeper bubble clouds, thicker foam layers are expected on the surface not only for stage A but also for stage B whitecaps. Therefore 10 GHz will feel increasingly more stage B whitecaps as wind speed increases. With thicker residual foam at higher wind speeds, 10 GHz could be expected to become more variable due to the larger influence of the secondary factors on the stage B whitecaps; this might explain the increased spread in the 10 GHz data.

Next, at the highest wind speeds, especially for W at 37 GHz, one can see some leveling off (saturation) of the satellite-based W, previously mentioned by Salisbury et al. (2013). A similar behavior was seen with the in situ W data described in the work by Callaghan et al. (2008). At higher wind speeds, the surface becomes quite complex with bubbles, foam, and spray, which might be a precursor of so called whiteout conditions as discussed by Holthuijsen et al. (2012). This leveling off in the whitecap fraction, similar to the leveling off of the drag coefficient (e.g., Zweers et al., 2010; Holthuijsen et al., 2012), is intriguing and deserves further analysis. However, before claiming physical reasons for this feature, an extended scrutiny of the $W(T_B)$ algorithm is needed to rule out modeling causes.

Finally, it was found that residual W decreases with increasing temperature (Sect. 3.1; Fig. 7). A similar observation was reported by Bortkovskii and Novak (1993) as a result of an increase in the life-time of foam patches with decreasing SST which was explained through an increase in bubble life-time for colder waters. This is in contrast to their reported effect on W of viscosity, which is increasing with decreasing temperature (Monahan and O'Muircheartaigh, 1986), and was found to reduce wave breaking activity and consequently to reduce the ocean surface fraction covered by foam patches. Another factor that is confirmed to affect the life-time of residual W is the presence of surfactants at the ocean surface (Callaghan, 2013) which are more abundant at lower temperatures due to higher primary production (Falkowski et al., 1998), which increases bubble life-time and thus extends the life-time of residual foam (Salisbury et al., 2013). In a recent laboratory study by Callaghan et al. (2014), the existence of an effect of water temperature on air entrainment and bubble plumes was confirmed. These authors concluded that the reported effects are far less significant compared to other factors affecting W, like e.g. wave field characteristics.

4.2 $W(U_{10})$-parameterization

4.2.1 Derivation of the new $W(U_{10})$ parameterization

From the assessment of the W data with respect to variations on regional scales, the influence of secondary factors, in addition to U_{10}, on W seems to be imbedded in the exponent of the wind speed dependence. It should therefore be reasonable to derive a W parameterization as a function of U_{10} as it is simple enough for global modeling applications yet it incorporates the natural variability of whitecap fraction.

In the derivation of the $W(U_{10})$ parameterization it was chosen to plot the square root of W against U_{10} to weigh both axes evenly. Because the resulting scatterplots shaped up linearly, linear fits were applied to these scatterplots which, by simply squaring the average of the best linear fits, led to the final parameterization with a quadratic polynomial form. Summarizing the results of all regions by calculating the average did not lead to a significantly different parameterization as was derived from the global data and it is therefore safe to use the global parameterization for global applications. However, when applying W on a regional scale it should be preferred to use a regionally derived parameterization, since the differences between the regional parameterizations could be substantial as illustrated in Fig. 5f.

Salisbury et al. (2013) mention several references that provide a strong theoretical basis supporting a cubic relationship, but the same arguments can also be used in

Discussion Paper | Discussion Paper | Discussion Paper | Discussion Paper |

ACPD
15, 21219–21269, 2015

Parameterization of oceanic whitecap fraction based on satellite observations

M. F. M. A. Albert et al.

favor of the quadratic relationship as found in this study (Eq. 9). It has been argued that W should be proportional to the energy flux supplied by wind which is proportional to the cube of the friction velocity u_* resulting in a cubic $W(u_*)$ and above cubic $W(U_{10})$ parameterizations (Wu, 1988). However, whitecaps are suppressed by swell (Sugihara et al., 2007; Salisbury et al., 2013) and thus not all of the energy that is supplied to waves is dissipated through breaking waves and whitecap formation, but instead some energy is used to oppose swell conditions. This might explain the lower (quadratic) wind exponent derived in this paper, especially considering that on a global scale swell conditions are dominant over wind sea conditions (Salisbury et al., 2013). It should also be noted that many in situ data are obtained in regions dominated by sea wind conditions (coastal regions or regions with a limited fetch), which should be kept in mind when comparing in situ studies with the work in this study.

To quantify the possible intrinsic correlation in the derived $W(U_{10})$ parameterization (Eq. 9), we have used ECMWF wind speeds instead of the QuikSCAT wind speeds (Sect. 2.3). We evaluate two aspects of the W, $U_{10\mathrm{QSCAT}}$, and $U_{10\mathrm{ECMWF}}$ data used to obtain the $W(U_{10})$ relationship. One aspect is that $U_{10\mathrm{ECMWF}}$ values are about 5 % lower than $U_{10\mathrm{QSCAT}}$ (Fig. 8a and Eq. 8). This 5 % difference for the U_{10} values up to 20 m s^{-1} leads to a difference in the whitecap fraction values of up to 8.5 %. The U_{10} differences between QuikSCAT and ECMWF can be explained to some extent with the effect of atmospheric stability because QuikSCAT provides equivalent neutral wind which accounts for the stability effects on the wind profile (Kara et al., 2008), while the ECMWF model gives stability dependent wind speeds (Chelton and Freilich, 2005). Another aspect is to evaluate the significance of the intrinsic correlation by looking at the change of the correlation coefficient of the $W(U_{10})$ relationship when QSCAT winds are substituted with the ECMWF winds. Physically, we expect a strong correlation between $\sqrt{W}$ and U_{10}, and we see this clearly in Fig. 4 which shows a squared correlation coefficient of $R^2 = 0.956$ for $\sqrt{W}$ and $U_{10\mathrm{QSCAT}}$. However, the correlation coefficient might not be as high as in Fig. 4 if U_{10} is from a more independent source. We show this in Fig. 8b which is similar to Fig. 4 but uses $U_{10\mathrm{ECMWF}}$. The $\sqrt{W(U_{10})}$ correlation is still clearly

ACPD
15, 21219–21269, 2015

seen in Fig. 8b, but the plot shows more scatter and the squared correlation coefficient is $R^2 = 0.826$. The slopes in Figs. 4 and 8b differ by up to 10 %, a difference comparable to that of using neutral and non-neutral wind speeds. The final $W(U_{10})$ parameterization given with Eq. (9) was obtained by combining Eqs. (7) and (8). However, due to rounding of the coefficients of the combined equation the final result is equal to the square of Eq. (7), which means that the impact of Eq. (8) is lost in the process. We have checked the error that is introduced by the rounding and found that it leads to an underestimate of W ranging from −6.5 % at $U_{10} = 3\,\mathrm{m\,s^{-1}}$ to ~ −10 % at $U_{10} = 20\,\mathrm{m\,s^{-1}}$. Of course, we have to consider these differences in the light of other uncertainties in the parameterization such as the goodness of the relationship between $U_{10\mathrm{QSCAT}}$ and $U_{10\mathrm{ECMWF}}$ and the satellite-based W data itself. We do not have a good estimate of neither of this at the moment. We therefore conclude that the effect of the intrinsic correlation on W, is presumed to lie within the error margins of the final $W(U_{10})$ parameterization given with Eq. (9).

For completeness, we have also investigated the effect of either rising or waning winds on the $W(U_{10})$ relationship. Although the value of W has been observed to be somewhat higher for waning than for rising winds, these differences are not statistically relevant. An effect of the wind history, therefore, is not included in the resulting $W(U_{10})$ parameterization (Eq. 9).

The rise-wane (undeveloped-developed sea) effect as detected in this study is not very pronounced compared to findings in studies that use in situ wind speed data (Stramska and Petelski, 2003; Callaghan et al., 2008; Goddijn-Murphy et al., 2011). Goddijn-Murphy et al. (2011) studied wind history- and wave development dependences on in situ W data using either ECMWF wave model data, QuikSCAT satellite data, or in situ data for U_{10}. These authors only detected significant effects with in situ data for U_{10}. The absence of a significant wind history effect in this study might therefore be traced back to the method through which U_{10} was determined: wind speeds from satellites are spatial averages of scatterometric or radiometric observations that take a snapshot of the surface as it is affected by both history and local conditions,

ACPD
15, 21219–21269, 2015

whereas in situ data for wind speed are single point values averaged over a short time and hence representative for a relatively small area. The effect of the spatial averaging of the satellite data over a much larger area (i.e. the satellite footprint) might be that information on wind history is lost in the process.

4.2.2 Comparison with other functional relationships

In Fig. 12 the parameterization derived in this study (Eq. 9) is compared to $W(U_{10})$ parameterizations obtained by MOM80, Callaghan et al. (2008), and Salisbury et al. (2013). The differences between the MOM80 parameterization and Eq. (9) are discussed in Sect. 3.2. Note that in most studies, as in this study, MOM80 is extrapolated beyond the range of the data from which this parameterization was derived (Monahan, 1971; Toba and Chaen, 1973). Therefore, at higher wind speeds the W values that are obtained using the MOM80 parameterization are somewhat questionable. At the same time, the QuikSCAT instrument that provided the U_{10} satellite data that are used in this study has a decreased sensitivity for wind speeds over $20\,\mathrm{m\,s^{-1}}$ (Quilfen et al., 2007). All results regarding higher wind speeds should therefore be handled with caution.

The analyses in this study can be considered to complement the work of Salisbury et al. (2013, 2014) who also analysed satellite-based whitecap fraction data but with a different approach. These authors considered effects on W from a selection of quantities additional to U_{10} on a global scale, whereas in this study it was tried to visualize and identify effects of additional variables by comparing W data sets in different regions. Salisbury et al. (2013) report dependency of W on secondary factors up to 25 %. On this basis, Salisbury et al. suggest to expand the W database with additional variables responsible for these effects to better quantify W variability. By using a kind of top down approach, implicitly including all additional variables, this study comes to a different conclusion regarding the use of W on a global scale: when all unspecified additional factors are included by using them implicitly, they seem to average out or to be sufficiently covered by the exponent of the $W(U_{10})$ parameterization as discussed in Sect 3.1.2, and in this sense it is not necessary to include additional variables.

There is little difference between the $W(U_{10})$ parameterizations derived by Salisbury et al. (2013) (Eq. 1) and Eq. (9) derived here (Fig. 12). While on one hand this is to be expected because these parameterizations are based on similar data sets, it is noteworthy that different analyses and parameterization approaches produced similar wind exponents, pointing to the robustness of the derived $W(U_{10})$ relationship. Differences that do occur can be explained by the somewhat different use of the same data. For example, in this study all available W data are included in the analyses, while Salisbury et al. (2013) removed W data with a relative standard deviation $(\sigma_W/W) > 2$, which was about 10 % of all W estimates, mostly in regions with low wind speeds of around $3\,\mathrm{m\,s^{-1}}$, around the onset of foam formation.

Because differences with the alternative $W(U_{10})$ parameterization derived by Callaghan et al. (2008) (Fig. 12) were previously discussed by Salisbury et al. (2013) and the differences between Eq. (9) and the Salisbury et al. (2013) parameterization have turned out to be rather insignificant, we refer to this latter study for a detailed comparison.

However, a final remark can be made considering the method of obtaining W data, either from satellite, as in this study and the study from Salisbury et al. (2013), or in situ as in MOM80 and Callaghan et al. (2008). Callaghan et al. (2008) report a change in slope in $W^{1/3}$ as function of U_{10} at wind speeds of around $10\,\mathrm{m\,s^{-1}}$. These authors suggest that the change in the dependence of W on U_{10} might indicate a different interaction between wind and waves, due to the onset of spume droplet production between 9 and $11\,\mathrm{m\,s^{-1}}$. Another explanation was provided by Goddijn-Murphy et al. (2011) who suggest the appearance of underdeveloped waves at higher wind speeds, resulting in lower W values. Because in their study Callaghan et al. (2008) used video images that were taken from a research vessel, whereas in this study data are obtained from satellite, and no changes in slope can be perceived, this might also point at an effect of the measurement method. One might speculate on an effect of wind direction compared to

ACPD
15, 21219–21269, 2015

Parameterization of oceanic whitecap fraction based on satellite observations

M. F. M. A. Albert et al.

the direction in which the research vessel is moving. The emissivity of a breaking wave does have azimuthal dependence (Wentz, 1992). Considering the position of a vessel in higher winds facing waves that increase in height with increasing U_{10}, it is plausible that W could be underestimated. The reported change in slope might then coincide with a certain wave height above which this underestimation exists.

4.3 Sea spray emission estimate

When modeling SSA emission, the impact of the modeling method used can be quite significant; e.g., Lewis and Schwartz (2004) report a spread in global emission estimates based on the M86 SSSF (Eq. 4), resulting from different studies, ranging from 3.3×10^{12} to $11.7 \times 10^{12}\,\mathrm{kg\,yr^{-1}}$, mainly caused by differences in model input data and resolution differences (Grythe et al., 2014). Also, Table 2 in the work by de Leeuw et al. (2011) shows examples of the use of the same SSA production method leading to significantly different results when applied in a different model. The two estimates made in this study, obtained with the M86 SSSF, including either the original MOM80 or the newly derived Eq. (9) $W(U_{10})$ parameterization (Sect. 3.3), are calculated using the same modeling tool and input data. Similarly, Grythe et al. (2014) used the same model simulation to evaluate 21 SSSFs, including M86, against measurements. We thus can put our new estimate into perspective by comparing our results to those found in the Grythe et al. (2014, their Table 2) study. In the comparison, we scale the deviation between our and the Grythe et al. (2014) model using M86. Specifically, using M86, Grythe et al. (2014) report two SSA emissions: an SSA estimate of $4.51 \times 10^{12} \pm 0.44\,\mathrm{kg\,yr^{-1}}$ for the size range of $0.8\,\mu\mathrm{m} < r_{80} < 8\,\mu\mathrm{m}$, where the estimated value is a 25 year average with an inter-annual variability range of ±0.44, and an SSA emission of $5.20 \times 10^{12} \pm 0.50\,\mathrm{kg\,yr^{-1}}$ for size range of $0.1\,\mu\mathrm{m} < r_{80} < 10\,\mu\mathrm{m}$ (referred to as M86E in Grythe et al., 2014). With regard to the size range, note that the contribution of the mass of submicron particles with $D_\mathrm{p} < 1\,\mu\mathrm{m}$ to the total mass of particles with $D_\mathrm{p} < 10\,\mu\mathrm{m}$ is not substantial (in the order of 1 %) (Facchini et al., 2008). These Grythe et al. estimates are about 1.5 times larger than the estimate of

ACPD
15, 21219–21269, 2015

$2.9 \times 10^{12}\,\mathrm{kg\,yr^{-1}}$ found in this study using our modeling tool (Sect. 2.4) with M86 and MOM80. This factor of 1.5 can then be applied to the SSA emission estimate that we obtained with the new $W(U_{10})$ parameterization (Eq. 9), resulting in a "model corrected" value of $6.2 \times 10^{12}\,\mathrm{kg\,yr^{-1}}$. Comparison of this value to the Grythe et al. estimates shows that our estimate is in the lower range of the reported global annual mass emissions, roughly 3×10^{12}–$70 \times 10^{12}\,\mathrm{kg\,yr^{-1}}$. This model corrected value is also of the same order as the estimates of the Sofiev et al. (2011) SSSFs, and the Grythe et al. (2014) SSSF (also reported in Table 2 of Grythe et al., 2014).

The original Sofiev et al. (2011) SSSF is based on the M86 SSSF combined with experimental data from laboratory experiments by Mårtensson et al. (2003) and a field experiment by Clarke et al. (2006) to increase the validity range but also to account for SST and salinity effects. However, in the work by Grythe et al. (2014) the salinity weight proposed by Sofiev et al. (2011) is not applied, resulting in an SSA emission estimate of $2.59 \times 10^{12} \pm 0.33\,\mathrm{kg\,yr^{-1}}$, at a reference salinity of 33 ‰ (referred to as S11T in Grythe et al., 2014). Grythe et al. (2014) also calculated an SSA emission estimate from the Sofiev et al. (2011) SSSF, leaving out temperature dependence, resulting in an estimate of $5.87 \times 10^{12} \pm 0.57\,\mathrm{kg\,yr^{-1}}$, at a reference salinity of 33 ‰ and a reference temperature of 25 °C (referred to as S11 in Grythe et al., 2014). The Grythe et al. (2014) S11 estimate is, as expected, close to the M86E estimate. Including temperature dependence, a lower estimate was found (S11T). In contrast, our estimate is assumed to implicitly account for temperature and salinity dependence through the $W(U_{10})$ parameterization, and results in a higher estimate compared to M86E. This cannot be caused by inclusion of salinity dependence because the fixed reference salinity is that of the oceans, and including varying salinities almost exclusively includes lower salinity values, resulting in lower emission estimates. This thus suggests that other secondary factors affecting W in a different way are far more important than temperature resulting in a net increase of our emission estimate. This suggestion is supported by results from the work of Salisbury et al. (2013) who found that, after wind

ACPD
15, 21219–21269, 2015

speed, the most important secondary factor that accounts for variability in W is the wavefield.

The Grythe et al. (2014) SSSF was obtained by modifying the Smith and Harrison (1998) SSSF, based on observational data, by adding an extra lognormal mode to cover the accumulation mode and including temperature dependence. The SSA emission estimate that was obtained using this SSSF ($8.91 \times 10^{12} \pm 0.61\,\mathrm{kg\,yr^{-1}}$) was, compared to the other reviewed source functions by Grythe et al. (2014), found to be closest to the observations considered in the same work, and only about 1.5 times higher compared to our new satellite-based estimate.

Our estimate is also close to those produced by the general circulation model KYU with sea salt emission estimates based on empirical wind speed dependent surface concentration equations derived by Erickson et al. (1986) (Takemura et al., 2000), and the chemical transport model UMI with SSA production method as described in Gong et al. (1997), 3.9×10^{12} and $3.8 \times 10^{12}\,\mathrm{kg\,yr^{-1}}$, respectively (see Fig. 1 of de Leeuw et al., 2011; Textor et al., 2006). As in our study, KYU and UMI models considered particles with a maximum r_{80} of $10\,\mu\mathrm{m}$. With similar size range but different modeling approaches, one may expect a variability in the range of the one reported by Lewis and Schwartz (2004) mentioned at the start of this section. However, not only the global annual production found in these two studies is close to our SSA estimate of $4.1 \times 10^{12}\,\mathrm{kg\,yr^{-1}}$, but also the global source flux distributions of these two models are comparable to those we report.

A recent study by Savelyev et al. (2014) suggests the use of brightness temperature polarization difference ΔT_{B}, to parameterize the production rate of SSA. These authors collected collocated measurements of concentrations of coarse mode aerosol originating from clean marine air, and measurements of surface brightness temperature with a microwave radiometer at a frequency of 10.7 GHz, both horizontally and vertically polarized, aboard the Floating Instrument Platform (FLIP) in the open Pacific Ocean. The measured concentrations were converted to SSA surface fluxes using dry deposition and vertical gradient methods. These authors found a strong correlation be-

ACPD
15, 21219–21269, 2015

tween the SSA surface flux and ΔT_B. The derived relationship between the SSA flux and ΔT_B presented the SSA flux better than U_{10}. Therefore, these authors suggest that a parameterization in terms of ΔT_B might be preferred over U_{10} to determine the SSA production rate. Savelyev et al. (2014) use both H and V polarization, whereas in our study, for reasons mentioned in Sect. 2.2, only H polarized data are considered. Anguelova et al. (2006) mentioned that W affects both H and V polarizations. In the light of Savelyev et al. (2014) results, it seems the use of both H and V polarization to determine W (and then SSA) is well warranted. In the calculation of our SSA emission estimate, we have chosen to only use the 37 GHz data set. However, if we would have used 10 GHz data instead, these would have been more representative of thicker foam layers and the V polarization data would probably have been more important. However, due to the different stages of whitecap formation that are visualised by the 10 GHz frequency data, these would to some extent be representative of the generation of spume droplets and cover mainly bubble-mediated jet- and film drops generation in the initial stage of whitecap formation.

In the recent works by Norris et al. (2013) and Ovadnevaite et al. (2014), SSSFs were parameterized in terms of the Reynolds number instead of the commonly used U_{10}, which resulted in better agreement with in situ measurements. Such results are consistent with the finding of Salisbury et al. (2013) that a wind-wave Reynolds number is causing almost as much variability in W as U_{10}. Supported by the results of Savelyev et al. (2014), the works of Norris et al. (2013) and Ovadnevaite et al. (2014) point to a new trend in describing SSA emissions with parameters different from U_{10}. The work described in this study seems to blend well in this new direction.

5 Conclusions

The study presented here aimed at improving the accuracy of a whitecap-method based sea spray source function (SSSF) by reducing the uncertainties in the parameterization of W. The approach was based on a satellite-based data set containing W

ACPD
15, 21219–21269, 2015

data estimated from measurements of the ocean surface brightness temperature T_B by satellite-borne radiometers at two frequencies (10 and 37 GHz), together with matching environmental and statistical data for 2006.

A global assessment of the data set to evaluate the wind speed dependence of W revealed a quadratic correlation between W and U_{10}. The relatively large spread in the 37 GHz data set, as compared to that at 10 GHz, could be attributed to secondary factors affecting W in addition to U_{10}. A regional scale assessment to better visualize effects of these secondary factors shows that the influence of secondary factors on wind speed dependences of W across retrieval frequency, season, or location apparently averages out or is imbedded in the exponent of the wind speed dependence. The high correlation coefficients between W and U_{10} support this conclusion and leaves little room to explain the effects of other possible drivers. However, with the 37 GHz data set the absolute values of W were different in different regions and seasons. This result has implications for collecting W data with the purpose of capturing and parameterizing the natural variability of whitecap formation and extent. The 10 GHz data set hardly showed any variability, neither in the wind speed dependences, nor in the absolute values. This leads to the plausible conclusion that new foam formation is less, if at all, affected by varying secondary environmental factors.

A whitecap fraction W parameterization was derived as a function of U_{10} only, as it is simple enough for global modeling applications yet it incorporates the natural variability of whitecap fraction. A possible intrinsic correlation between W and U_{10}, which could have been introduced while estimating W from T_B, was evaluated by using a more independent U_{10} source, $U_{10\text{ECMWF}}$. The $U_{10\text{ECMWF}}$ values were found to be about 5 % lower than $U_{10\text{QSCAT}}$ (Fig. 8a and Eq. 8). This 5 % difference for U_{10} values up to 20 m s^{-1} leads to differences in whitecap fraction values of up to 8.5 %. This leads to the conclusion that the effect of the intrinsic correlation on W is presumed to lie within the error margins of the final $W(U_{10})$ parameterization. Also, the effect of wind history on the $W(U_{10})$ relationship was examined and was found to be relatively insignificant, and was not further considered. A new $W(U_{10})$ parameterization for global application with a quadratic correlation between W and U_{10} was developed and compared to previously derived $W(U_{10})$ parameterizations. Because most existing parameterizations have cubic and higher wind speed dependences and the most abundant wind speeds are generally below $15\,\mathrm{m\,s^{-1}}$, the quadratic $W(U_{10})$ parameterization derived in this study will most of the time lead to higher W estimates than obtained from the cubic or higher correlations.

Application of the $W(U_{10})$ parameterization in the Monahan et al. (1986) SSSF resulted in a total supermicron SSA mass emission estimate of 4082 Tg (4.1×10^{12} kg) for 2006, which is comparable to previously reported estimates.

Several recent studies were found to move towards SSSFs that use different parameters, other than U_{10}, which would better suit to describe SSA emissions. Considering our new $W(U_{10})$ parameterization that implicitly accounts for these different parameters, it is plausible that our approach using satellite-based W data to reduce the uncertainties in the parameterization of W, will help to improve future SSA emission estimates.

Data availability

The data analysis and the results reported in this study are available from the corresponding author M. F. M. A. (Monique) Albert (monique.albert@tno.nl).

Acknowledgements. This study is partly funded by SRON, Netherlands Institute for Space Research, through the Dutch Users Support Programme GO-2. MDA was sponsored by the Office of Naval Research, NRL Program element 61153N, WU 4500.

References

Albert, M. F. M. A., Schaap, M., de Leeuw, G., and Builtjes, P. J. H.: Progress in the determination of the sea spray source function using satellite data, Journal of Integrative Environmental Sciences, 7, 159–166, 2010.

Albert, M. F. M. A., Schaap, M., Manders, A. M. M., Scannell, C., O'Dowd, C. D., and de Leeuw, G.: Uncertainties in the determination of global sub-micron marine organic matter emissions, Atmos. Environ., 57, 289–300, 2012.
Andreae, M. O. and Crutzen, P. J.: Atmospheric aerosols: biogeochemical sources and role in atmospheric chemistry, Science, 276, 1052–1058, 1997.
Andreas, E. L.: Sea spray and the turbulent air–sea heat fluxes, J. Geophys. Res., 97, 11429–11441, 1992.
Anguelova, M. D. and Gaiser, P. W.: Skin depth at microwave frequencies of sea foam layers with vertical profile of void fraction, J. Geophys. Res., 116, C11002, doi:10.1029/2011JC007372, 2011.
Anguelova, M. D. and Gaiser, P. W.: Microwave emissivity of sea foam layers with vertically inhomogeneous dielectric properties, Remote Sens. Environ., 139, 81–96, 2013.
Anguelova, M. D. and Webster, F.: Whitecap coverage from satellite measurements: a first step toward modeling the variability of oceanic whitecaps, J. Geophys. Res., 111, C03017, doi:10.1029/2005JC003158, 2006.
Anguelova, M. D., Bettenhausen, M. H., and Gaiser, P. W.: Passive remote sensing of sea foam using physically-based models, in: Proceedings of the IGARSS 2006: IEEE International Geoscience and Remote Sensing Symposium, Denver, Colorado, USA, 31 July–4 August, 3659–3662, 2006.
Anguelova, M. D., Bobak, J. P., Asher, W. E., Dowgiallo, D. J., Moat, B. I., Pascal, R. W., and Yelland, M. J.: Validation of satellite-based estimates of whitecap coverage: approaches and initial results, in: Proceedings of the 16th Air–Sea Interaction conference, AMS, Phoenix, Arizona, USA, 10–15 January, 14 pp., 2009.
Asher, W. E. and Wanninkhof, R.: The effect of bubble-mediated gas transfer on purposeful dual-gaseous tracer experiments, J. Geophys. Res., 103, 10555–10560, 1998.
Barrie, L. A., Bottenheim, J. W., Schnell, R. C., Crutzen, P. J., and Rasmussen, R. A.: Ozone destruction and photochemical reactions at polar sunrise in the lower Arctic atmosphere, Nature, 334, 138–141, 1988.
Bettenhausen, M. H., Smith, C. K., Bevilacqua, R. M., Wang, N.-Y., Gaiser, P. W., and Cox, S.: A nonlinear optimization algorithm for WindSat wind vector retrievals, IEEE T. Geosci. Remote, 44, 597–610, 2006.
Blanchard, D. C.: The electrification of the atmosphere by particles from bubbles in the sea, Prog. Oceanogr., 1, 73–112, 1963.

ACPD
15, 21219–21269, 2015

Parameterization of oceanic whitecap fraction based on satellite observations

M. F. M. A. Albert et al.

Blanchard, D. C.: The production, distribution, and bacterial enrichment of the sea-salt aerosol, in: Air–Sea Exchange of Gases and Particles, edited by: Liss, P. S. and Slinn, W. G. N., D. Reidel Publishing Company, Dordrecht, the Netherlands, 407–454, 1983.

Bortkovskii, R. S. and Novak, V. A.: Statistical dependencies of sea state characteristics on water temperature and wind-wave age, J. Marine Syst., 4, 161–169, 1993.

Callaghan, A. H.: An improved whitecap timescale for sea spray aerosol production flux modeling using the discrete whitecap method, J. Geophys. Res.-Atmos., 118, 9997–10010, 2013.

Callaghan, A. H. and White, M.: Automated processing of sea surface images for the determination of whitecap coverage, J. Atmos. Ocean. Tech., 26, 383–394, 2009.

Callaghan, A. H., de Leeuw, G., Cohen, L., and O'Dowd, C. D.: Relationship of oceanic whitecap coverage to wind speed and wind history, Geophys. Res. Lett., 35, L23609, doi:10.1029/2008GL036165, 2008.

Callaghan, A. H., Stokes, M. D., and Deane, G. B.: The effect of water temperature on air entrainment, bubble plumes, and surface foam in a laboratory breaking-wave analog, J. Geophys. Res.-Oceans, 119, 7463–7482, 2014.

Chameides, W. L. and Stelson, A. W.: Aqueous-phase chemical processes in deliquescent sea-salt aerosols: a mechanism that couples the atmospheric cycles of S and sea salt, J. Geophys. Res.-Atmos., 97, 20565–20580, 1992.

Chelton, D. B. and Freilich, M. H.: Scatterometer-based assessment of 10-m wind analyses from the operational ECMWF and NCEP numerical weather prediction models, Mon. Weather Rev., 133, 409–429, 2005.

Cicerone, R. J.: Halogens in the atmosphere, Rev. Geophys. Space Ge., 19, 123–139, 1981.

Clarke, A. D., Owens, S. R., and Zhou, J.: An ultrafine sea-salt flux from breaking waves: implications for cloud condensation nuclei in the remote marine atmosphere, J. Geophys. Res., 111, D06202, doi:10.1029/2005JD006565, 2006.

de Leeuw, G., Andreas, E. L., Anguelova, M. D., Fairall, C. W., Lewis, E. R., O'Dowd, C. D., Schulz, M., and Schwartz, S. E.: Production flux of sea spray aerosol, Rev. Geophys., 49, RG2001, doi:10.1029/2010RG000349, 2011.

Erickson, D. J., Merrill, J. T., and Duce, R. A.: Seasonal estimates of global atmospheric sea-salt distributions, J. Geophys. Res.-Atmos., 91, 1067–1072, 1986.

Facchini, M. C., Rinaldi, M., Decesari, S., Carbone, C., Finessi, E., Mircea, M., Fuzzi, S., Ceburnis, D., Flanagan, R., Nilsson, E. D., de Leeuw, G., Martino, M., Woeltjen, J., and

O'Dowd, C. D.: Primary submicron marine aerosol dominated by insoluble organic colloids and aggregates, Geophys. Res. Lett., 35, L17814, doi:10.1029/2008GL034210, 2008.
Fairall, C. W., Kepert, J. D., and Holland, G. J.: The effect of sea spray on surface energy transports over the ocean, The Global Atmosphere and Ocean System, 2, 121–142, 1994.
Falkowski, P. G., Barber, R. T., and Smetacek, V.: Biogeochemical controls and feedbacks on ocean primary production, Science, 281, 200–206, 1998.
Gaiser, P. W., St. Germain, K. M., Twarog, E. M., Poe, G. A., Purdy, W., Richardson, D., Grossman, W., Linwood Jones, W., Spencer, D., Golba, G., Cleveland, J., Choy, L., Bevilacqua, R. M., and Chang, P. S.: The WindSat spaceborne polarimetric microwave radiometer: sensor description and early orbit performance, IEEE T. Geosci. Remote, 42, 2347–2361, 2004.
Garrett, W. D.: Stabilization of air bubbles at the air–sea interface by surface-active material, Deep-Sea Res., 14, 661–672, 1967.
Ghan, S. J., Guzman, G., and Hayder, A.-R.: Competition between sea salt and Sulfate particles as cloud condensation nuclei, J. Atmos. Sci., 55, 3340–3347, 1998.
Goddijn-Murphy, L., Woolf, D. K., and Callaghan, A. H.: Parameterizations and algorithms for oceanic whitecap coverage, J. Phys. Oceanogr., 41, 742–756, 2011.
Gong, S. L., Barrie, L. A., and Blanchet, J. -P.: Modeling sea-salt aerosols in the atmosphere 1. Model development, J. Geophys. Res., 102, 3805–3818, 1997.
Graedel, T. E. and Keene, W. C.: The budget and cycle of Earth's natural chlorine, Pure Appl. Chem., 68, 1689–1697, 1996.
Grythe, H., Ström, J., Krejci, R., Quinn, P., and Stohl, A.: A review of sea-spray aerosol source functions using a large global set of sea salt aerosol concentration measurements, Atmos. Chem. Phys., 14, 1277–1297, doi:10.5194/acp-14-1277-2014, 2014.
Hanson, J. L. and Phillips, O. M.: Wind sea growth and dissipation in the open ocean, J. Phys. Oceanogr., 29, 1633–1648, 1999.
Holthuijsen, L. H., Powell, M. D., and Pietrzak, J. D.: Wind and waves in extreme hurricanes, J. Geophys. Res., 117, C09003, doi:10.1029/2012JC007983, 2012.
Kara, A. B., Wallcraft, A. J., and Bourassa, M. A.: Air–sea stability effects on the 10 m winds over the global ocean: evaluations of air–sea flux algorithms, J. Geophys. Res.-Oceans, 113, C04009, doi:10.1029/2007JC004324, 2008.

ACPD
15, 21219–21269, 2015

Parameterization of oceanic whitecap fraction based on satellite observations

M. F. M. A. Albert et al.

Keene, W. C., Pszenny, A. A. P., Jacob, D. J., Duce, R. A., Galloway, J. N., Schultz-Tokos, J. J., Sievering, H., and Boatman, J. F.: The geochemical cycling of reactive chlorine through the marine troposphere, Global Biogeochem. Cy., 4, 407–430, 1990.

Keene, W. C., Khalil, M. A. K., Erickson, D. J., McCulloch, A., Graedel, T. E., Lobert, J. M., Aucott, M. L., Gong, S.-L., Harper, D. B., Kleiman, G., Midgley, P., Moore, R. M., Seuzaret, C., Sturges, W. T., Benkovitz, C. M., Koropalov, V., Barrie, L. A., and Li, Y.-F.: Composite global emissions of reactive chlorine from anthropogenic and natural sources: reactive chlorine emissions inventory, J. Geophys. Res., 104, 8429–8440, 1999.

Kleiss, J. M. and Melville, W. K.: The analysis of sea surface imagery for whitecap kinematics, J. Atmos. Ocean. Tech., 28, 219–243, 2011.

Koop, T., Kapilashrami, A., Molina, L. T., and Molina, M. J.: Phase transitions of sea-salt/water mixtures at low temperatures: implications for ozone chemistry in the polar marine boundary layer, J. Geophys. Res., 105, 26393–26402, 2000.

Lewis, E. R. and Schwartz, S. E.: Sea Salt Aerosol Production: Mechanisms, Methods, Measurements and Models – a Critical Review, Geoph. Monog. Series, 152, American Geophysical Union, Washington D.C., USA, 413 pp., 2004.

Luria, M. and Sievering, H.: Heterogeneous and homogeneous oxidation of SO_2 in the remote marine atmosphere, Atmos. Environ. A-Gen., 25, 1489–1496, 1991.

Mårtensson, E. M., Nilsson, E. D., de Leeuw, G., Cohen, L. H., and Hansson, H.-C.: Laboratory simulations and parameterization of the primary marine aerosol production, J. Geophys. Res., 108, 4297, doi:10.1029/2002JD002263, 2003.

Medwin, H.: In situ acoustic measurements of microbubbles at sea, J. Geophys. Res., 82, 971–976, 1977.

Meissner, T. and Wentz, F. J.: The emissivity of the ocean surface between 6 and 90 GHz over a large range of wind speeds and earth incidence angles, IEEE T. Geosci. Remote, 50, 3004–3026, 2012.

Melville, W. K.: The role of surface-wave breaking in air–sea interaction, Annu. Rev. Fluid Mech., 28, 279–321, 1996.

Monahan, E. C.: Oceanic whitecaps, J. Phys. Oceanogr., 1, 139–144, 1971.

Monahan, E. C. and O'Muircheartaigh, I.: Optimal power-law description of oceanic whitecap coverage dependence on wind speed, J. Phys. Oceanogr., 10, 2094–2099, 1980.

Monahan, E. C. and O'Muircheartaigh, I.: Whitecaps and the passive remote sensing of the ocean surface, Int. J. Remote Sens., 7, 627–642, 1986.

ACPD
15, 21219–21269, 2015

Monahan, E. C. and Woolf, D. K.: Comments on "Variations of whitecap coverage with wind stress and water temperature", J. Phys. Oceanogr., 19, 706–709, 1989.
Monahan, E. C., Fairall, C. W., Davidson, K. L., and Boyle, P. J.: Observed inter-relations between 10 m winds, ocean whitecaps and marine aerosols, Q. J. Roy. Meteor. Soc., 109, 379–392, 1983.
Monahan, E. C., Spiel, D. E., and Davidson, K. L.: A model of marine aerosol generation via whitecaps and wave disruption, in: Oceanic Whitecaps and Their Role in Air–Sea Exchange Processes, edited by: Monahan, E. C. and Mac Niocaill, G., D. Reidel Publishing Company, Dordrecht, the Netherlands, 167–174, 1986.
Norris, S. J., Brooks, I. M., and Salisbury, D. J.: A wave roughness Reynolds number parameterization of the sea spray source flux, Geophys. Res. Lett., 40, 4415–4419, 2013.
O'Dowd, C. D. and de Leeuw, G.: Marine aerosol production: a review of the current knowledge, Philos. T. R. Soc. A, 365, 1753–1774, 2007.
O'Dowd, C. D., Lowe, J. A., Smith, M. H., and Kaye, A. D.: The relative importance of non-sea-salt sulphate and sea-salt aerosol to the marine cloud condensation nuclei population: an improved multi-component aerosol-cloud droplet parametrization, Q. J. Roy. Meteor. Soc., 125, 1295–1313, 1999.
O'Dowd, C. D., Facchini, M. C., Cavalli, F., Ceburnis, D., Mircea, M., Decesari, S., Fuzzi, S., Yoon, Y. J., and Putaud, J.-P.: Biogenically driven organic contribution to marine aerosol, Nature, 431, 676–680, 2004.
Ovadnevaite, J., Manders, A., de Leeuw, G., Ceburnis, D., Monahan, C., Partanen, A.-I., Korhonen, H., and O'Dowd, C. D.: A sea spray aerosol flux parameterization encapsulating wave state, Atmos. Chem. Phys., 14, 1837–1852, doi:10.5194/acp-14-1837-2014, 2014.
Pandey, P. C. and Kakar, R. K.: An empirical microwave emissivity model for a foam-covered sea, IEEE J. Oceanic Eng., 7, 135–140, 1982.
Partanen, A.-I., Dunne, E. M., Bergman, T., Laakso, A., Kokkola, H., Ovadnevaite, J., Sogacheva, L., Baisnée, D., Sciare, J., Manders, A., O'Dowd, C., de Leeuw, G., and Korhonen, H.: Global modelling of direct and indirect effects of sea spray aerosol using a source function encapsulating wave state, Atmos. Chem. Phys., 14, 11731–11752, doi:10.5194/acp-14-11731-2014, 2014.
Quilfen, Y., Prigent, C., Chapron, B., Mouche, A. A., and Houti, N.: The potential of QuikSCAT and WindSat observations for the estimation of sea surface wind vector under severe weather conditions, J. Geophys. Res., 112, C09023, doi:10.1029/2007JC004163, 2007.

ACPD
15, 21219–21269, 2015

Parameterization of oceanic whitecap fraction based on satellite observations

M. F. M. A. Albert et al.

Saiz-Lopez, A. and von Glasow, R.: Reactive halogen chemistry in the troposphere, Chem. Soc. Rev., 41, 6448–6472, 2012.
Salisbury, D. J., Anguelova, M. D., and Brooks, I. M.: On the variability of whitecap fraction using satellite-based observations, J. Geophys. Res.-Oceans, 118, 6201–6222, 2013.
Salisbury, D. J., Anguelova, M. D., and Brooks, I. M.: Global distribution and seasonal dependence of satellite-based whitecap fraction, Geophys. Res. Lett., 41, 1616–1623, 2014.
Savelyev, I. B., Anguelova, M. D., Frick, G. M., Dowgiallo, D. J., Hwang, P. A., Caffrey, P. F., and Bobak, J. P.: On direct passive microwave remote sensing of sea spray aerosol production, Atmos. Chem. Phys., 14, 11611–11631, doi:10.5194/acp-14-11611-2014, 2014.
Sievering, H., Boatman, J., Gorman, E., Kim, Y., Anderson, L., Ennis, G., Luria, M., and Pandis, S.: Removal of sulphur from the marine boundary layer by ozone oxidation in sea-salt aerosols, Nature, 360, 571–573, 1992.
Sievering, H., Gorman, E., Ley, T., Pszenny, A., Springer-Young, M., Boatman, J., Kim, Y., Nagamoto, C., and Wellman, D.: Ozone oxidation of sulfur in sea-salt aerosol particles during the Azores Marine Aerosol and Gas Exchange experiment, J. Geophys. Res.-Atmos., 100, 23075–23081, 1995.
Smith, M. H. and Harrison, N. M.: The sea spray generation function, J. Aerosol Sci., 29, S189–S190, 1998.
Sofiev, M., Soares, J., Prank, M., de Leeuw, G., and Kukkonen, J.: A regional-to-global model of emission and transport of sea salt particles in the atmosphere, J. Geophys. Res., 116, D21302, 2011.
Stramska, M. and Petelski, T.: Observations of oceanic whitecaps in the north polar waters of the Atlantic, J. Geophys. Res., 108, 3086, doi:10.1029/2002JC001321, 2003.
Sugihara, Y., Tsumori, H., Ohga, T., Yoshioka, H., and Serizawa, S.: Variation of whitecap coverage with wave-field conditions, J. Marine Syst., 66, 47–60, 2007.
Takemura, T., Okamoto, H., Maruyama, Y., Numaguti, A., Higurashi, A., and Nakajima, T.: Global three-dimensional simulation of aerosol optical thickness distribution of various origins, J. Geophys. Res., 105, 17853–17873, 2000.
Textor, C., Schulz, M., Guibert, S., Kinne, S., Balkanski, Y., Bauer, S., Berntsen, T., Berglen, T., Boucher, O., Chin, M., Dentener, F., Diehl, T., Easter, R., Feichter, H., Fillmore, D., Ghan, S., Ginoux, P., Gong, S., Grini, A., Hendricks, J., Horowitz, L., Huang, P., Isaksen, I., Iversen, I., Kloster, S., Koch, D., Kirkevåg, A., Kristjansson, J. E., Krol, M., Lauer, A., Lamarque, J. F., Liu, X., Montanaro, V., Myhre, G., Penner, J., Pitari, G., Reddy, S., Seland, Ø., Stier, P.,

ACPD
15, 21219–21269, 2015

Takemura, T., and Tie, X.: Analysis and quantification of the diversities of aerosol life cycles within AeroCom, Atmos. Chem. Phys., 6, 1777–1813, doi:10.5194/acp-6-1777-2006, 2006.
Thorpe, S. A.: On the clouds of bubbles formed by breaking wind-waves in deep water, and their role in air–sea gas transfer, Philos. T. R. Soc. S.-A, 304, 155–210, 1982.
Toba, Y. and Chaen, M.: Quantitative expression of the breaking of wind waves on the sea surface, in: Records of Oceanographic Works in Japan, 12, National Research Council of Japan, Tokyo, 1–11, 1973.
Wanninkhof, R., Asher, W. E., Ho, D. T., Sweeney, C., and McGillis, W. R.: Advances in quantifying air–sea gas exchange and environmental forcing, Annual Review of Marine Science, 1, 213–244, 2009.
Wentz, F. J.: A model function for ocean microwave brightness temperatures, J. Geophys. Res., 88, 1892–1908, 1983.
Wentz, F. J.: Measurement of oceanic wind vector using satellite microwave radiators, IEEE T. Geosci. Remote, 30, 960–972, 1992.
Wentz, F. J.: A well-calibrated ocean algorithm for special sensor microwave/imager, J. Geophys. Res., 102, 8703–8718, 1997.
Woolf, D. K.: Bubbles and their role in gas exchange, in: The Sea Surface and Global Change, edited by: Liss, P. S. and Duce, R. A., Cambridge Univ. Press, New York, 173–205, 1997.
Wu, J.: Variations of whitecap coverage with wind stress and water temperature, J. Phys. Oceanogr., 18, 1448–1453, 1988.
Zhao, D. and Toba, Y.: Dependence of whitecap coverage on wind and wind-wave properties, J. Oceanogr., 57, 603–616, 2001.
Zweers, N. C., Makin, V. K., de Vries, J. W., and Burgers, G.: A sea drag relation for hurricane wind speeds, Geophys. Res. Lett., 37, L21811, doi:10.1029/2010GL045002, 2010.

ACPD
15, 21219–21269, 2015

Table 1. Coordinates, number of data points, range and mean value for wind speed, and range and mean value of SST of selected regions (a) for January 2006, (b) for July 2006.

Region	Lon.	Lat.	Number of samples	Wind speed [$m\,s^{-1}$] Range	Mean	SST [°C] Range	Mean
a							
1. Gulf of Mexico	86–95° W	23–28° N	19 472	1.3–15.7	7.5	19.4–26	23.8
2. S. Atlantic Ocean	1–15° W	1–30° S	173 288	0.2–12.9	6.4	21.4–27.8	24.2
3. Indian Ocean	75–89° E	1–30° S	179 496	0.03–13.4	7.0	23.0–29.4	26.8
4. N. Atlantic Ocean	11–20° W	30–44° N	51 672	0.2–19.6	8.0	13.3–20.4	16.4
5. S. Pacific Ocean	86–100° W	31–60° S	204 776	0.5–23.0	8.7	4.8–24.1	12.7
6. Pacific Ocean (equator)	171–180° W	15° S–14° N	125 352	0.6–15.6	8.2	26.2–30.4	28.4
7. N. Atlantic Ocean	31–50° W	10–29° N	92 808	0.3–15.0	8.8	20.1–27.9	24.9
b							
Region	Lon.	Lat.	Number of samples	Wind speed [$m\,s^{-1}$] Range	Mean	SST [°C] Range	Mean
1. Gulf of Mexico	86–95° W	23–28° N	17 096	0.4–10.0	4.5	28.7–30.5	29.5
2. S. Atlantic Ocean	1–15° W	1–30° S	196 544	0.2–14.0	6.6	17.7–27.1	23.2
3. Indian Ocean	75–89° E	1–30° S	198 408	0.6–15.4	8.0	18.8–30.0	25.4
4. N. Atlantic Ocean	11–20° W	30–44° N	45 592	0.7–14.0	6.7	16.9–23.3	20.4
5. S. Pacific Ocean	86–100° W	31–60° S	262 944	0.7–22.7	9.8	2.5–19.1	9.3
6. Pacific Ocean (equator)	171–180° W	15° S–14° N	143 064	0.09–14.8	6.0	26.9–29.7	28.8
7. N. Atlantic Ocean	31–50° W	10–29° N	89 928	0.4–13.6	7.4	23.6–28.0	26.0

ACPD
15, 21219–21269, 2015

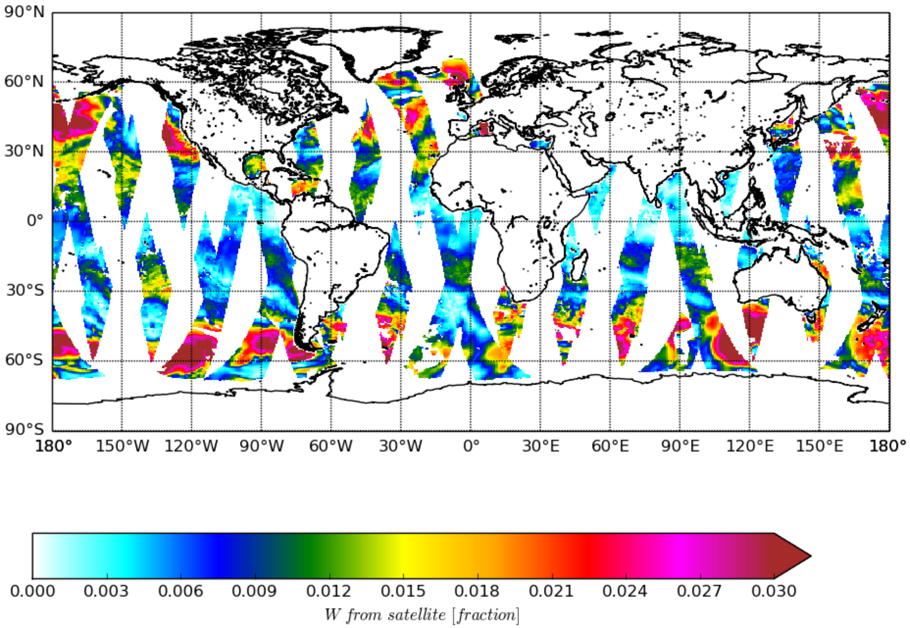

Figure 1. Satellite retrieved 37 GHz W data for 11 March 2006.

ACPD
15, 21219–21269, 2015

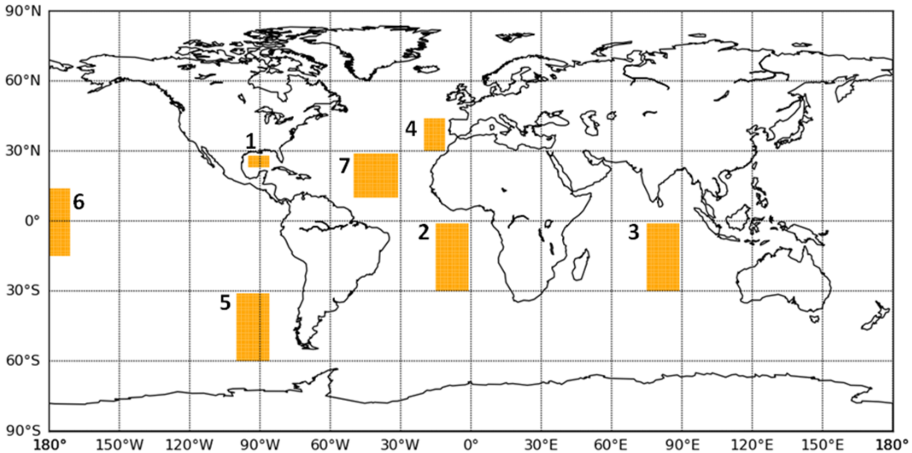

Figure 2. Selected regions to determine regional variations of $W(U_{10})$.

ACPD
15, 21219–21269, 2015

Parameterization of oceanic whitecap fraction based on satellite observations

M. F. M. A. Albert et al.

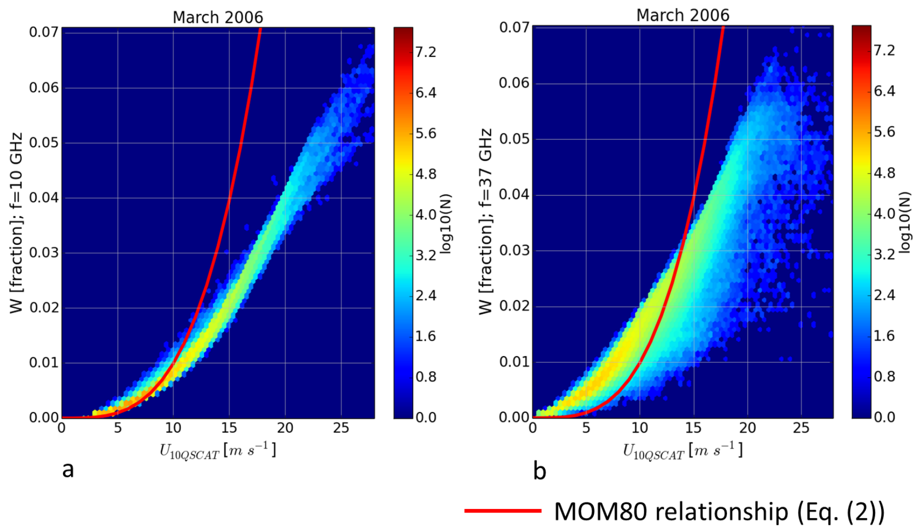

Figure 3. Global W as function of U_{10} from QuikSCAT for March 2006 where W is obtained with 10 GHz **(a)** – and 37 GHz **(b)** measurement frequency. The colors indicate the amount of data points per hexabin.

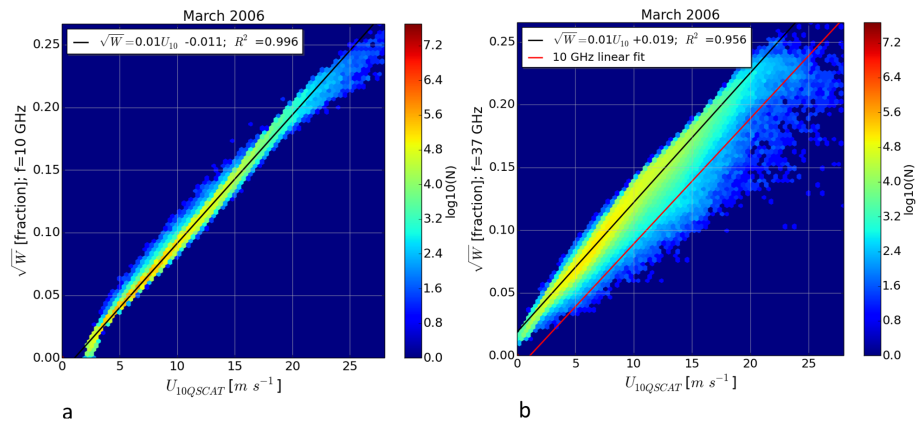

Figure 4. Global $\sqrt{W}$ as function of U_{10} from QuikSCAT for March 2006, where $\sqrt{W}$ is obtained with 10 GHz **(a)** – and 37 GHz **(b)** measurement frequency. The black line (in both panels) indicates the best linear fit through the data. The red line in the right panel equals the black line in the left panel. The colors indicate the amount of data points per hexabin.

ACPD
15, 21219–21269, 2015

Parameterization of oceanic whitecap fraction based on satellite observations

M. F. M. A. Albert et al.

Title Page
Abstract | Introduction
Conclusions | References
Tables | Figures
◂◂ | ▸▸
◂ | ▸
Back | Close
Full Screen / Esc
Printer-friendly Version
Interactive Discussion

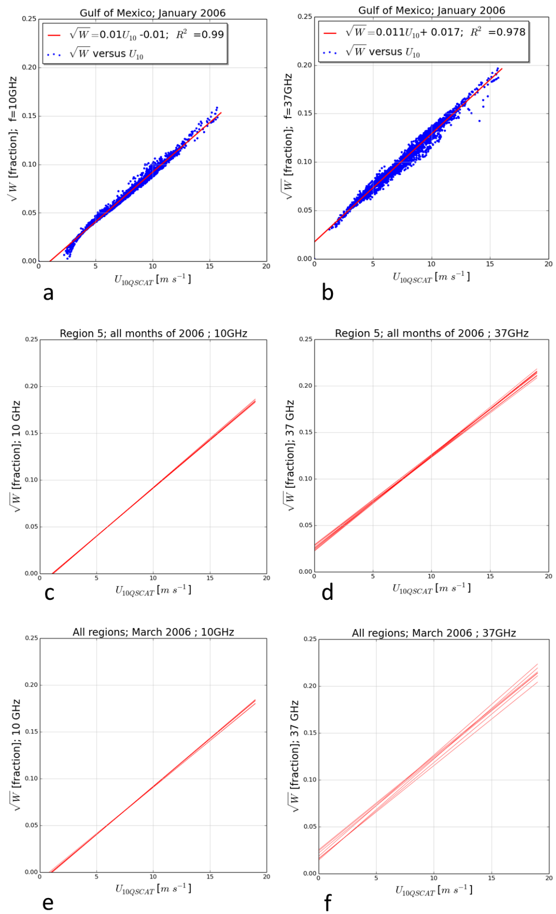

Figure 5. $\sqrt{W}$ vs. U_{10}: scatterplots with linear fits for region 1 for January 2006 at 10 GHz **(a)** and 37 GHz **(b)**; linear fits for region 5 for all months at 10 GHz **(c)** and 37 GHz **(d)**; linear fits for regions 1–7 for March 2006 at 10 GHz **(e)** and 37 GHz **(f)**.

ACPD
15, 21219–21269, 2015

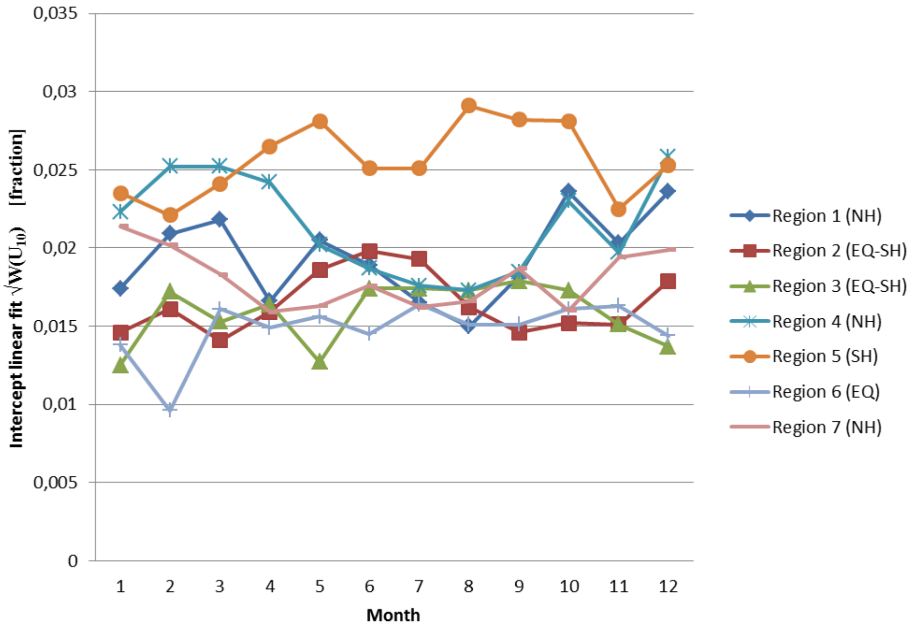

Figure 6. Regional and seasonal dependency of the $\sqrt{W(U_{10})}$ parameterizations' y intercept for all months of 2006. Regions as defined in Table 1. NH = Northern Hemisphere; EQ = Equator; SH = Southern Hemisphere.

ACPD
15, 21219–21269, 2015

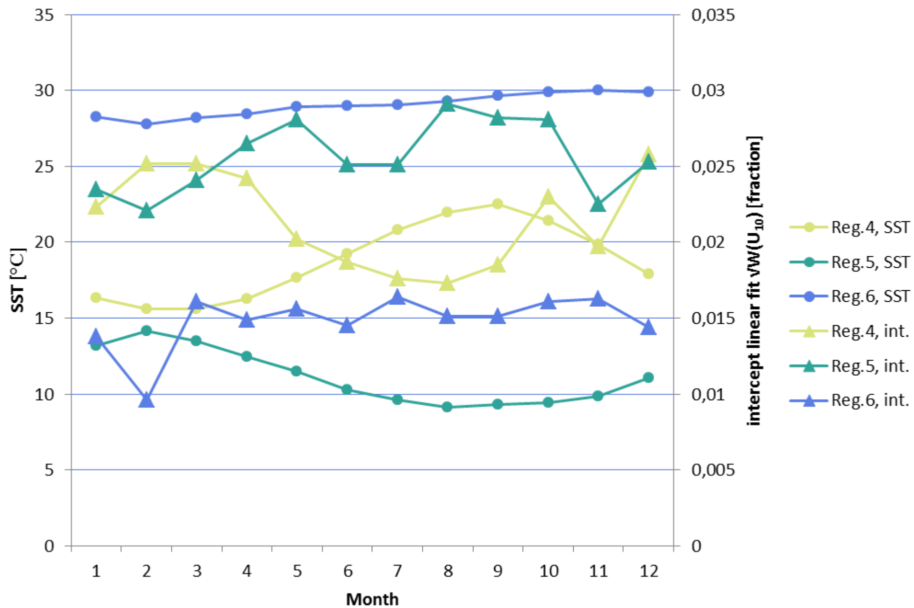

Figure 7. SST – (dots, left vertical axis) and intercept variability of the linear $\sqrt{W(U_{10})}$ parameterization (triangles, right vertical axis) for 2006 for three selected regions as defined in Table 1.

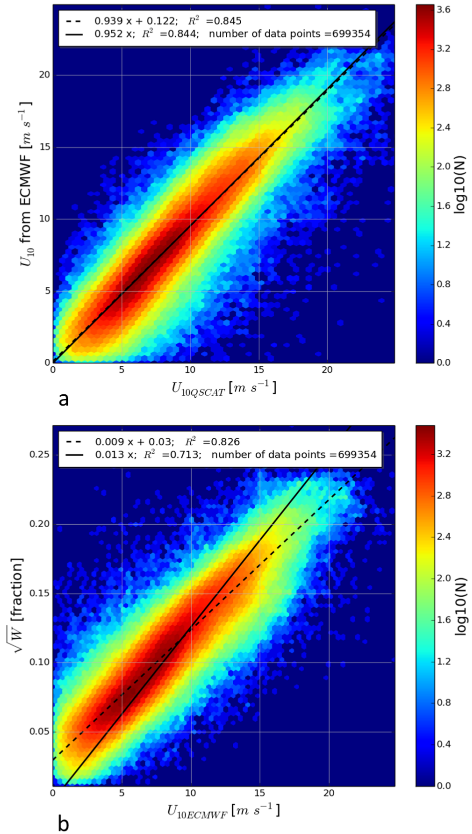

Figure 8. Intrinsic correlation between W and U_{10} from QuikSCAT. **(a)** Scatterplot of global $U_{10\mathrm{ECMWF}}$ vs. $U_{10\mathrm{QSCAT}}$ for March 2006. **(b)** Scatterplot of $\sqrt{W}$ vs. $U_{10\mathrm{ECMWF}}$ for March 2006. In both figures the colors indicate the amount of data points per hexabin. The black lines are linear fits: the dashed line represents the best fit and the solid line the best linear fit forced through zero. Values for R^2 are indicated.

ACPD
15, 21219–21269, 2015

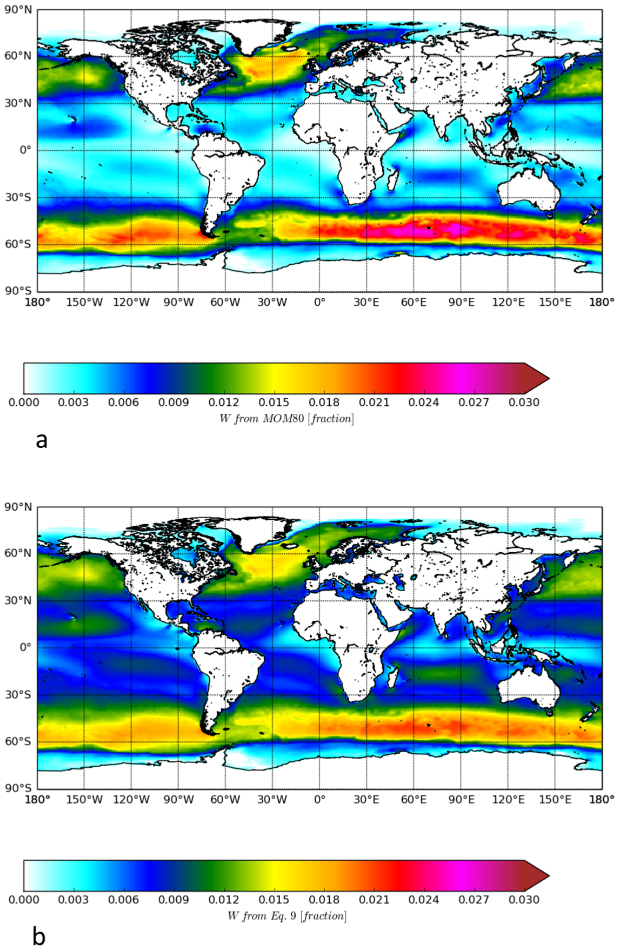

Figure 9. Annual average W distribution for 2006 calculated from the MOM80 $W(U_{10})$ parameterization (Eq. 2) **(a)** and from Eq. (9) **(b)**. U_{10} is extracted from the ECMWF data base.

ACPD
15, 21219–21269, 2015

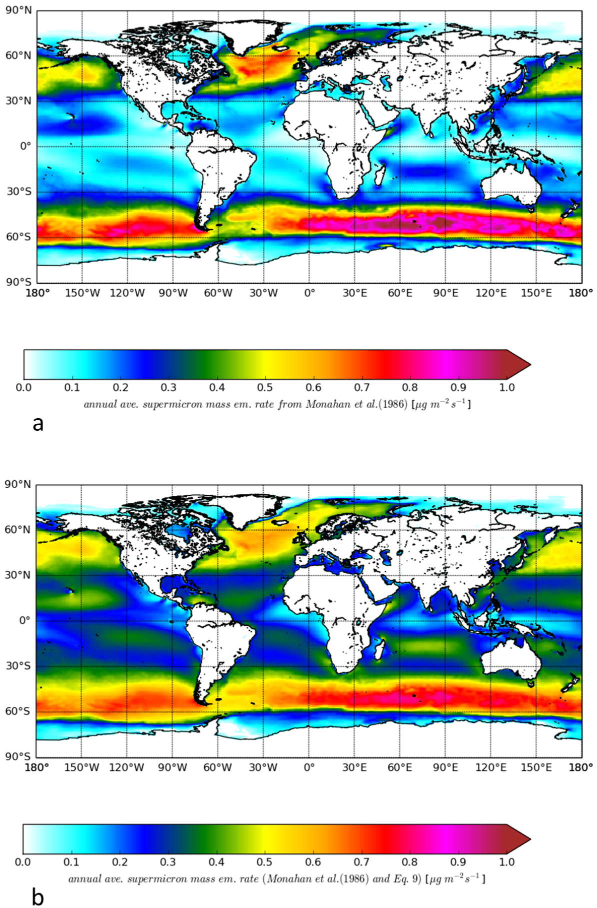

Figure 10. Annual average super micron mass emission rate for 2006 in $\mu g\, m^{-2}\, s^{-1}$ calculated from the MOM80 $W(U_{10})$ parameterization (Eq. 2) **(a)** and from Eq. (9) **(b)**. U_{10} is extracted from the ECMWF data base.

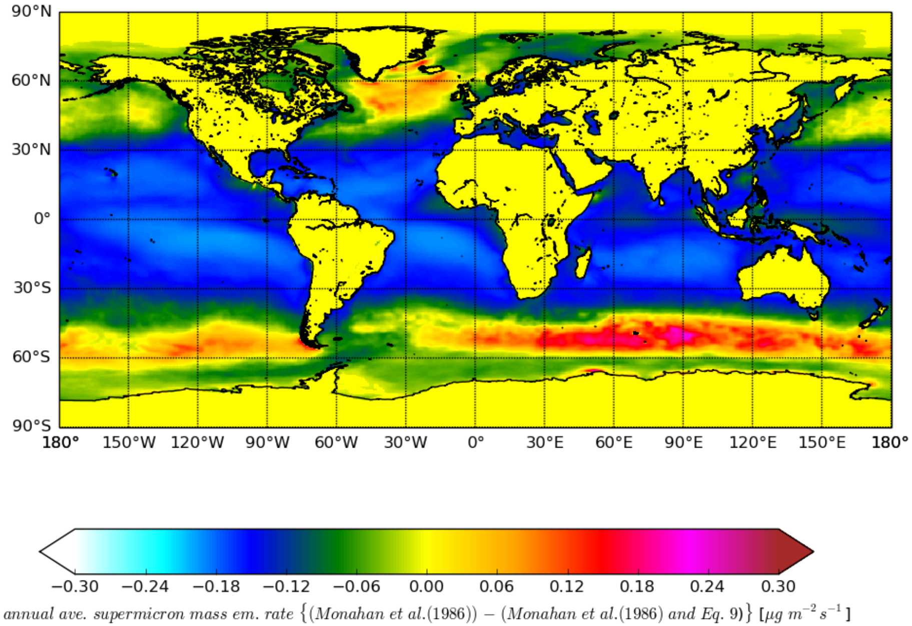

Figure 11. Difference between the annual average coarse mode SSA mass emission rate calculated from the Monahan et al. (1986) SSSF and the annual average coarse mode SSA mass emission rate calculated from the Monahan et al. (1986) SSSF where *W* is replaced with Eq. (9). Emission rates are calculated for 2006 in $\mu g\,m^{-2}\,s^{-1}$. U_{10} is extracted from the ECMWF data base.

ACPD
15, 21219–21269, 2015

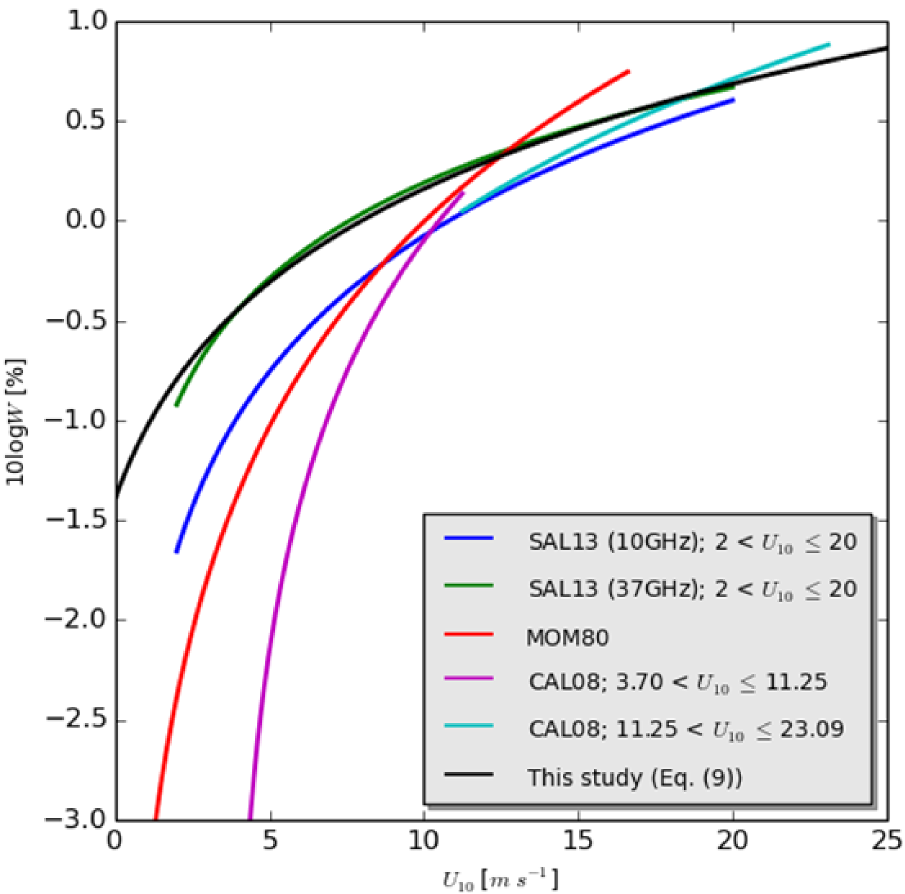

Figure 12. $W(U_{10})$ from different studies, where SAL13 (10 GHz) and SAL13 (37 GHz) are parameterizations from Salisbury et al. (2013) (Eq. 1), and CAL08 are parameterizations derived by Callaghan et al. (2008) (Eq. 3).

ACPD
15, 21219–21269, 2015

Parameterization of oceanic whitecap fraction based on satellite observations

M. F. M. A. Albert et al.